LUNDS UNIVERSITET

Silk's sweet spot: untangling the requirements for artificial silk extrusion using a biomimetic approach

Rodrigo Sanches Pires

Thesis submitted in partial fulfilment for the degree of Master of Science in Biotechnology (2019)

Supervisor:
Dr. Cedric Dicko (Docent)

Soft and Complex Biomaterials group
Division of Pure and Applied Biochemistry (Avdelningen för Tillämpad Biokemi)
Faculty of Engineering (Lunds Tekniska Högskola, LTH)
Lunds Universitet

The cosmos is within us. We are made of star-stuff. We are a way for the universe to know itself.

— **Carl Sagan**, *Cosmos*

Table of contents

Abbreviations Page 3
Acknowledgments Page 4
Popular science summary Page 5

Chapter 1: Introduction
Silk injectability: a continuous and unresolved problem Page 6
The ideal injectable Page 7
Hypothesis statement Page 9

Chapter 2: Theory
2.1. Silk processing inside the glands Page 9
2.2. Fabrication of RSF-based (hydro)gels Page 10
2.3. Biomimetic acidification Page 11
2.4. Measuring the silk self-assembly process and gelation processes Page 12
2.5. Thioflavin T: a ubiquitous marker for assembly and aggregation Page 14

Chapter 3: Materials and methods
3.1. Factorial design and optimization Page 16
3.2. Materials Page 16
3.3. Silk fibroin regeneration Page 16
3.4. Fabrication of biomimetic silk gels Page 17
3.5. Extrusion studies Page 17
3.6. Large-strain indentation Page 18
3.7. Self-assembly kinetics Page 18
    3.7.1. Fluorescence spectroscopy Page 19
    3.7.2. Turbidity Page 20
3.8. Extrusion effects on gel secondary structure Page 20
3.9 pH measurement

Chapter 4: Results Page 21
4.1. Definition of damaged and undamaged gels Page 21
4.2. Silk extrusion and mechanical properties of pre-extruded gels Page 23
4.3. Structure of extruded and non-extruded gels ATR FT-IR Page 24
4.4. Self-assembly of pre-extruded gels Page 27

Chapter 5: Discussion Page 30
Conclusion Page 31
References Page 31
Supplementary materials Page 36

Abbreviations

RSF	Regenerated silk fibroin
ThT	Thioflavin T
ATR	Attenuated total reflectance
FT-IR	Fourier transform Infrared spectroscopy
UV-vis	Ultraviolet-visible spectroscopy
IF	Intrinsic fluorescence
IFE	Inner filter effect
C–C bond	Single carbon-carbon covalent bond
ECM	Extracellular matrix
GDL	Glucono-δ-lactone
LiBr	Lithium bromide
ANOVA	Analysis of variance

Acknowledgments

First and foremost, I would like to thank my supervisor, Dr. Cedric Dicko, for all the support and guidance given during my project. I have learned a lot from you and for that I am extremely grateful. Spiders, silkworms, and silks have been a passion of mine since a very young age. I can hardly believe I would have been more happy working in any other project. I would like to thank all the group elements at the Soft and Complex Biomaterials Lab, and especially to Dr. Betina Ferreira for being such a motherly figure, and to Dr. Milena Lopes for being an intrinsically special and exceptionally good friend.

I am eternally grateful to my family. Without you, this work would not have been possible. I want to dedicate this thesis to my parents, who have so hardly worked throughout their lives to provide me with the education and the financial means to achieve my dreams. Equally, this worked is also dedicated to my brother, whom I very sadly, due to the circumstances of my choices, have not been able to see growing up. Lastly, even though they are not aware of it, I want to acknowledge my puppy, Zeus, and my baby cat, Safira, for bringing and showing me an outlandishly diverse, but simple ways happiness and joy can be given.

Popular Science summary

Silks comprise one of the most fascinating group of natural materials. Spider silk, for instance, is the toughest natural fibre known to man. It is a very fine combination of stretchiness and strength that makes spider silks tougher than Kevlar, steel, and many other man-made polymers. Recently, an interest in using silks as biomedical materials has arisen, mostly due to the fact that they do not trigger an immune response, can degrade easily in the body, and that they provide a friendly environment for cells to grow. Despite all the hype in the biomedical field, only a few examples of *Bombyx mori* derived fibroin-hydrogels were reported to be injectable. Of these, none are truly biomimetic and are instead comprised of blends with scarce amounts of silk. Such is of critical level, as it limits the extension of silks to regenerative applications, like 3D-bioprinting, localized drug delivery, and many others. Such technical challenge can be understood as the fact that, in nature, silks are designed to be pultruded and spun, and are the product of 400 million years of evolution and natural selection towards a very cost-efficient spinning system. Although technically challenging, up to this point, only a few have considered the natural progressive acidification to which silk proteins are exposed before spinning. Of those few, none has considered the physiological limitations of the active silk-spinners, nor even what is the definition of a suitable extrusion. When it comes to the design of artificial silk extrusion systems, we considered those to be essential. Throughout this project, the reader will understand that, by using a novel biomimetic acidification to formulate silk hydrogels, and by extruding them at speeds relevant for injection applications, we have been able to successfully achieve an artificial extrusion of purely-made silk hydrogels, which is within the physiological limitations of the active silk-spinners (i.e.: provided silk spinning was an extrusion-dominated process, the animals would not die extruding our gels from their bodies). Adding to that, a silk concentration ideal for extrusion, called here the “silk’s sweet spot”, has also been discovered.

Our findings have important effects in the field of regenerative medicine and biofabrication, as silk hydrogels and injectable systems should then be targeted to be formulated and optimized at this specific *sweet spot concentration.* With this project, a very critical step in using silks as the ultimate biomedical material has been taken. Hopefully, new injectables and studies using silk-based systems will start targeting this optimal concentration, and significant achievements in the biomedical field should thus be soon seen.

Chapter 1: Introduction

Silk injectability: a continuous and unresolved problem

Despite all the hype in the biomedical field, only a few examples of *Bombyx mori* derived fibroin-hydrogels were reported to be injectable. Of all these injectable systems, none of them are truly biomimetic and are instead comprised of blends with limited amounts of silk. [1–9] Although it is true that much has been made of silk's remarkable properties to fabricate injectable gels, it is also true that only a few have considered the natural progressive acidification to which silk proteins are exposed before spinning. Of those few, none has considered the physiological limitations of the active silk-spinners, nor even what is the definition of a suitable extrusion. Contrarily, we consider those to be essential when designing extrusion systems artificially. Indeed, forced reeling of *B. mori* silkworms suggests that both the processing and the feedstock play a significant role in silk fibre properties. This notion provided the impetus for this work. We asked if those premises also extended to the design of bio-inspired artificial extrusion systems. We rationalized that, by mimicking the natural way silks are processed by the animal, and by optimizing gels for their best extrusion properties, we could obtain a biologically relevant artificial extrusion of silks.

First and foremost, we asked how we could define the biological relevance of a bio-inspired extrusion process. The *biologically-relevant extrusion domain* is thus defined as the set of conditions in which the requirements for artificial silk extrusion are within the physiological limitations of natural silk producers, while extruding feedstock at adequate speeds that mimic the common speeds arbitrarily used by humans when applying injection systems (0,0803-1,9 mm/s) [5,10–17] (fig. 1).

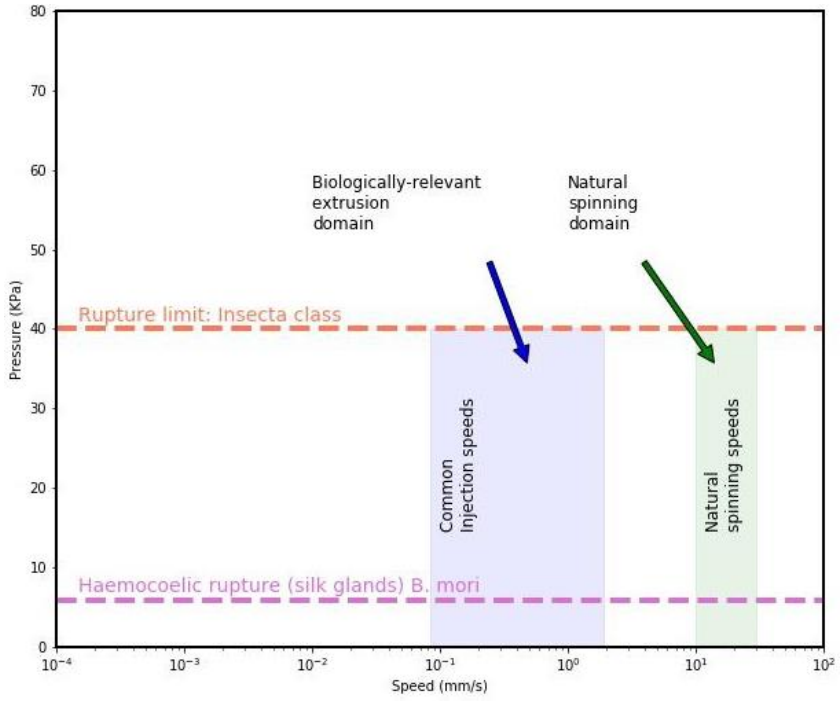

Fig. 1: Representation of the biological relevance for extrusion of silk gels at both natural spinning (*green area*) and common injection speeds (*blue area*) functionalized by the physiological limitations of the active-silk spinners.

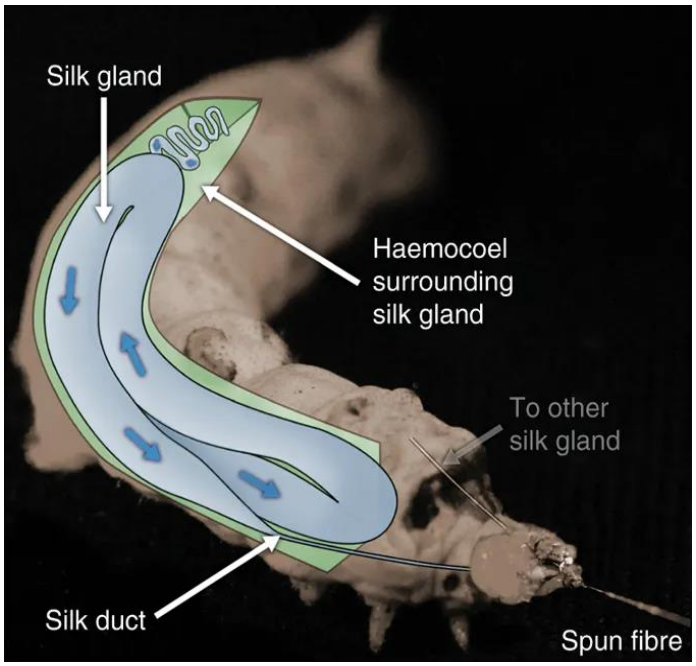

Fig. 2: Anatomical representation of the *Bombyx mori* silk gland and its silk-spinning apparatus. The gland (*blue*) surrounded by the haemocoel (*green*). The direction of silk flow during spinning is indicated by the blue arrows. Adapted from reference 74.

The physiological properties of natural spinners need to be considered for testing the relevance of the hypothesis. Even though the haemocoelic rupture pressure of final instar *B. mori* entering pupation is registered at 5,88 KPa [18] (fig. 2), recent work has shown that the spinning ducts of both *B.mori* and *N.clavipes* are reinforced with chitin in a way they would be less prone to deformation than the initial part of the glands. However, the maximum sustained pressure by these structures as never been recorded. A relevant analysis of the requirements for artificial extrusion cannot, nonetheless, be compared with haemocoelic rupture pressures of *B. mori*, as the animal is likely able to sustain much higher pressures around the spinning duct, which is where the spinning happens. A better upper limit for a relevant biological extrusion is thus delineated by the maximum internal pressures recorded in the *Insecta class*. In this case, 40 KPa for hard-bodied animals. [19–21] This is thus set as the limit in pressure the animals can sustain. Outside of this range, bio-inspired artificial extrusion has no biological meaning nor correlation to the natural spinning domain.

The ideal injectable system

An ideal extrudable matrix would require low force for the initial push, and a constant extrusion force (fig. 3 and 4) during the injection phase. A low initial push, followed by an equal-in-magnitude constant and non-noisy extrusion force profile, are direct signs that the pressure applied to initially move the gel did not cause cracking of the polymeric network. The idea of gel quality before and after extrusion is of great importance, as this will guide us to understand the quality of the extrusion.

The extrusion of fully-formed gels is categorized as follows:

(1) **Ideal**, where a constant, smooth and non-noisy flow of the gel is observed after the initial push.

(2) **Acceptable**, where the compressive forces during the initial push lead to a small drop in force.

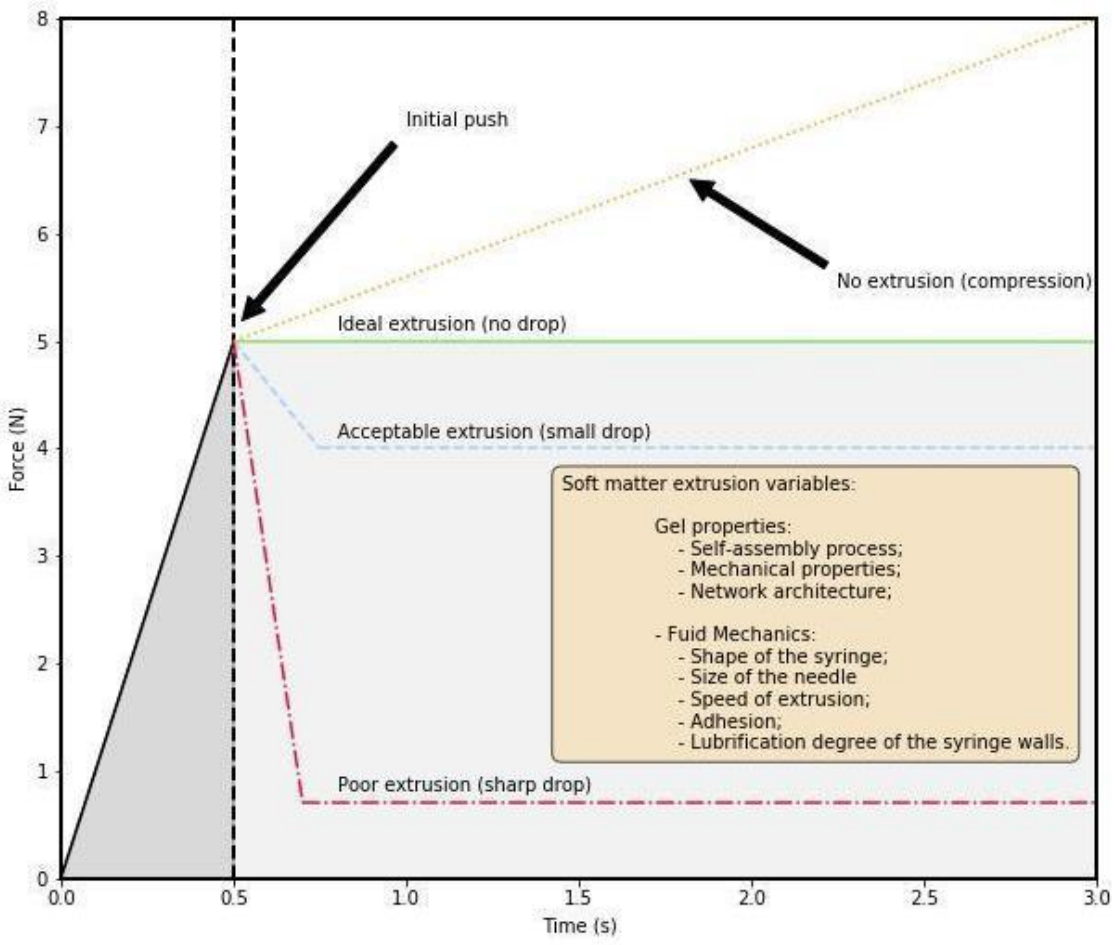

Fig. 3: Simplistic representation of the various possible extrusion profiles.

(3) **Poor**, where extrusion leads to complete fracture and prominent destruction of the gel network, either due to a high degree of water phase separation, or intensive gel fracturing.

(4) **Non-extrudable,** where the force applied on the gel by the plunger, is not sufficient to push the gel out.

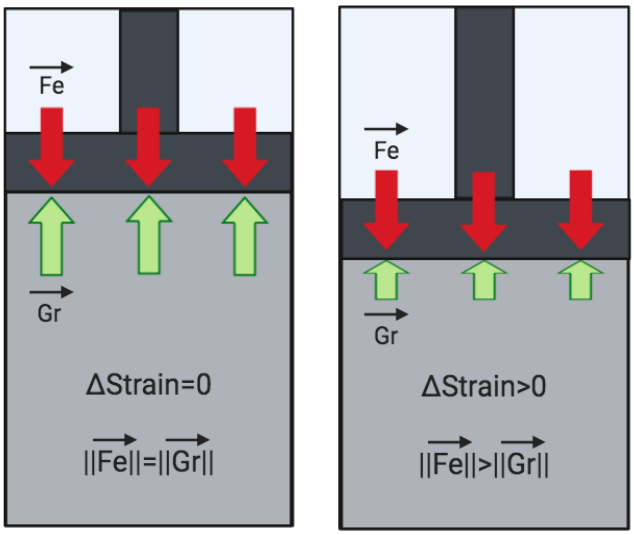

Fig. 4: Simplistic representation of the various dominating forces acting upon a non-extrudable (left), and extrudable gel (right). *Fe* represents the force exerted by the plunger to cause gel displacement (strain), and *Gr* is defined as the opposite resistance force to gel extrusion.

Following these definitions, we now thus have the base to ask the question, *can we reach a relevant artificial extrusion of silks by mimicking the way silk is processed and spun?*

Hypothesis statement

We hypothesized that artificial extrusion of silks and the overall improvement of their extrusion quality could be achieved by mimicking the natural way silk is processed.

Chapter 2: Theory

2.1. Silk processing inside the glands

Both spiders and silkworms produce silk inside designated structures named silk glands. These unique proteins are spun under ambient conditions with only water as their solvent [22–24]. Unlike spiders, the domesticated silkworm *Bombyx mori* produces large amounts of silk, and this silk is destined for cocoon building before pupation and metamorphosis from larvae to moths [22,25]. On the other hand, spiders spin different kinds of silk originating from different glands and part of their bodies, and they are destined for a variety of other different purposes than cocoon building in silkworms. [22–24,26]. Although different in molecular structure, both spider and silkworm silks are very long, highly repetitive, and extremely soluble proteins at high pH [22]. During silk production and spinning, a few peculiar notes can be made. Silk proteins are produced and stored at concentrations of about 30% wt. and then transported along a narrow tube where important secondary structural modifications occur (fig. 5), and which are mainly the response to a very mild pH gradient generated by proton pumps and carbonic anhydrase along the gland[22]. Indeed, this progressive acidification is responsible for protein refolding and beta-sheet transition from random coil

conformations, which is essential for spinning. [27,28] A great part of the evolutionary success of silks is hence related to these subtle natural treatments. In both insects [29,30] and spiders [31], the progressive acidification has been linked to dimerization of the silk proteins N-terminal domains; and, most likely yield an extension of the protein network to facilitate transport and tune the mechanical properties [32]
There is thus a great deal of importance in recreating these natural processing conditions when fabricating silk gels, as part of their success will also be dictated by the degree of mimicking that is used during their treatment.

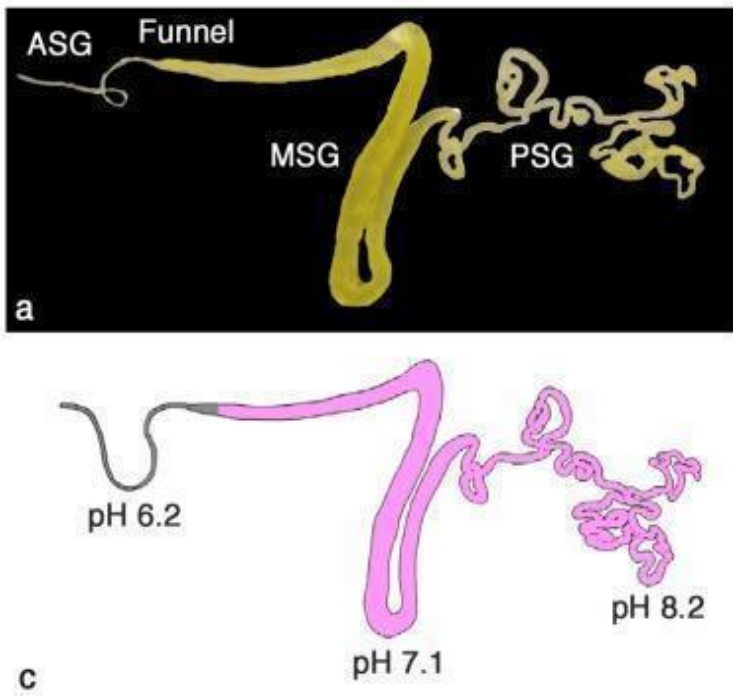

Fig. 5: (a) Silk gland extracted from *B. mori* with elucidation to the anterior, middle, and posterior silk gland (ASG, MSG, and PSG, respectively). Schematic representation (c) of the with pH values indicated in different parts depicting the progressive acidification inside the glands. Fibroin secreting parts are indicated in purple. Adapted from reference 22.

2.2. Fabrication of RSF-based (hydro)gels

When it comes to the biofabrication SF-based gels, a variety of different biofabrication approaches can be used. Gels can be formed via enzymatic cross-linking [7,33–37] or by encouraging physical entanglement of the biopolymers by either pH-driven [29], dehydration, or physical techniques. [38] Methods based on SF self-assembly via sonication[39], soft freezing [40], vortexing[3], electrogelation [41], dehydration [42], polyethylene oxide (PEO)[43] have been reported, amongst others. A wide variety of silk-blended gels can also be obtained. [1,2,44–47]

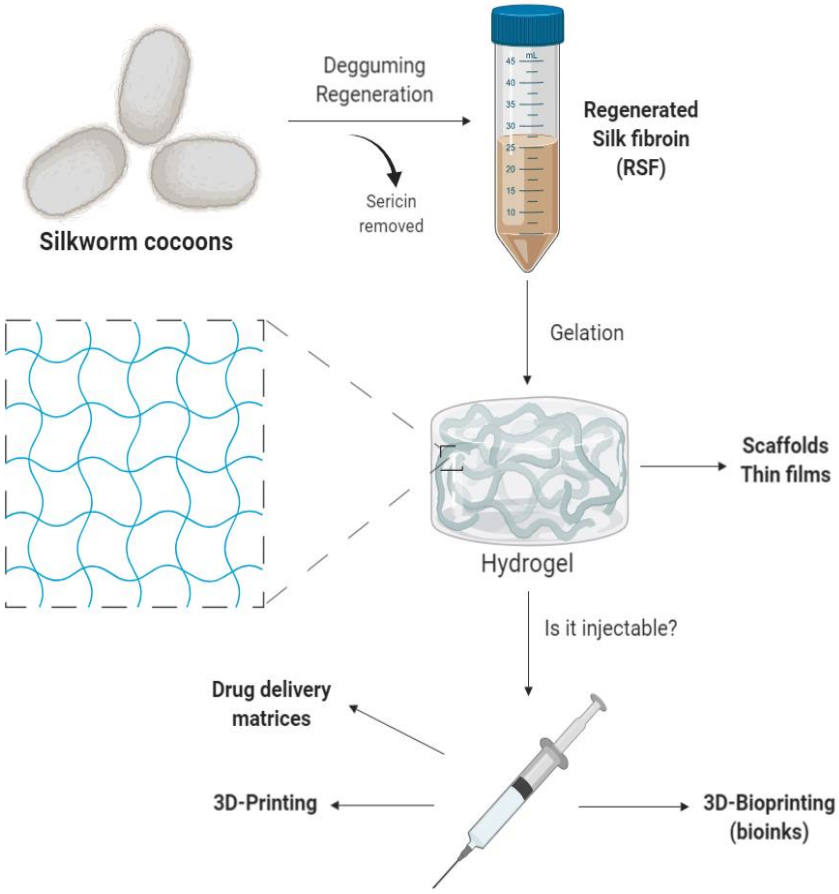

Fig. 6: Schematic workflow of the steps associated with silk (hydro)gel fabrication and its applications.

Fabrication of silk gels usually starts by removing the immunogenic sericin [48] . Here, sericin is separated from the fibroin portion of the silk fibres in the silkworm's cocoon (a process known as degumming [49]). After degumming the silk fibres, the sericin-free cocoons are dissolved into a viscous aqueous solution, what is known as regenerated silk fibroin (RSF). This step can be accomplished using a variety of different chemical and enzymatic methods [50,51] (a detailed overview of the degumming and regeneration processes, and their respective effects will not be given in this report. For details, please see references [49–53]). The RSF solution is then gelled, and the outcomes of assembled gels are summarized in figure 6. The problem with all of the current enumerated gelation protocols utilized for the fabrication of silk gels is that they fail to mimic the processing conditions found inside the animal's silk glands. In this report, a novel biomimetic acidification method based on the progressive acidification inside the glands of both spiders and silkworms will be used, as it is elucidated in the next section.

2.3. Biomimetic acidification

As previously referred, silk sol-to-gel transition based on pH-driven physical entanglement [27,28,54] is of high interest to employ. Silk self-assembly stimulated by acidic conditions is, of the current gelation approaches,

the one that more closely replicates the pH gradient and the way silk proteins are produced, stored, and transported inside the glands of both spiders and silkworms. [22,23] The technical challenges when designing a gelation protocol with a pH component is to provide a homogeneous change within all solution and throughout the entire gelation time. Mo et al. found that producing films by using acetic acid vapor worked to mimic natural acidification behaviour; however, formulation of gels with the same method is more demanding. More recently, high-pressure carbon dioxide has been used as volatile acid to induce pH-coupled gelation of aqueous silk solutions. [38] However, the considerably rapid change in pH and the bulky instrumentation provided by this method failed to recreate the natural acidification as it happens in the silk glands. The inherent problem with all of the present gelation procedures is that they do not successfully mimic the progressive acidification observed in the spinning apparatus. The novel method for the biomimetic gelation of silk used in this report is based on the progressive acidification created by the partial hydrolysis of glucono-δ-lactone (GDL) to gluconic acid, as described by the following reaction:

$$C_6H_{10}O_6 + H_2O \rightarrow C_6H_{12}O_7 \quad \text{(reaction 1).}$$

GDL is normally used as a food additive, sequestrant and or acidifier for milk oxidoreduction [55]
The use of progressive acidification gelation of silk is the extension of the work already performed in the acid unfolding of human serum albumin. [56]
This approach allows thus for the fabrication of silk-based hydrogels under biomimetic acidification, as it happens inside the animal's silk glands (fig. 7).

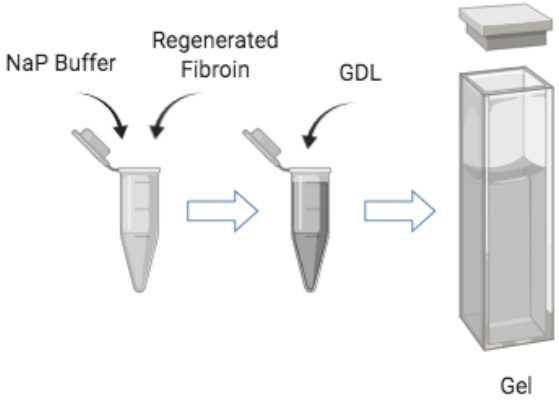

Fig. 7: Schematic representation of the progressive acidification method employed.

2.4. Measuring the silk self-assembly and gelation processes

Protein self-assembly refers to the natural and spontaneous supramolecular formation of highly organized protein structures. [57,58] These can include fibrils, amorphous aggregates, crystals, gels, and other architectures that can range from the nm to μm in size. For instance, (hydro)gels usually have a nano fibrillar nature and high-water content. They are due to be used as smart matrices to mimic the complex 3D topology

of native extracellular matrix (ECM). Silks, collagens, elastins, and prions are just some examples of biopolymers that can naturally self-assemble into "fibrils" and organized gel networks. [58]

Typically, self-assembly into fibrils can be captured by turbidity or fluorescence using a dye or scattering method. Figure 8 illustrates the process of self-assembly towards the gel state, as seen by turbidity measurement.

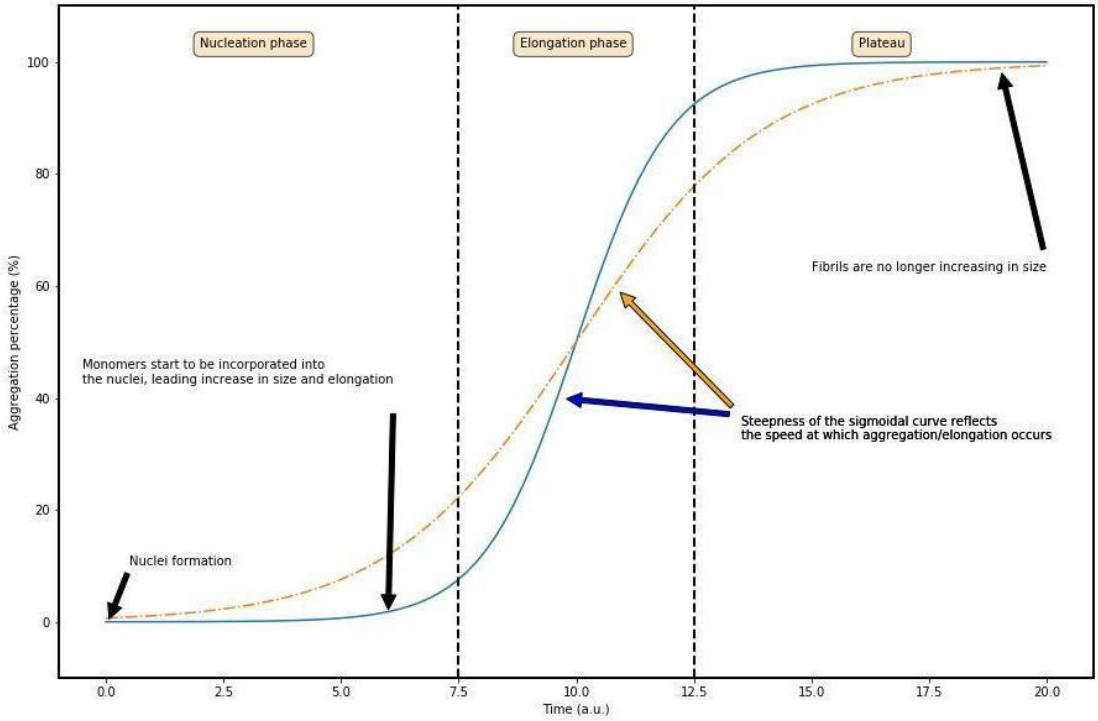

Fig. 8: Schematic representation of a characteristic macroscopic aggregation/elongation curve for fibril formation. The typical sigmoidal behaviour is noted in terms of aggregate concentration (in monomer equivalents, % of total monomer that as aggregated) as a function of time. Usually, sigmoidal transitions associated with fibrillar formation are divided into lag phase, an elongation phase, and a final plateau.

Self-assembly reactions, including silk sol-to-gel transition, typically display sigmoidal growth kinetics (fig. 8). [59] A defined sharp/steep transition zone is both preceded and followed by relatively flat regions, where no assemble into a gel network occurs (lag phase and plateau). During the elongation phase, structures grow in size, correlating to sol-to-gel transition, beta-sheet formation, and assemble into an organized gel network (fig. 9).

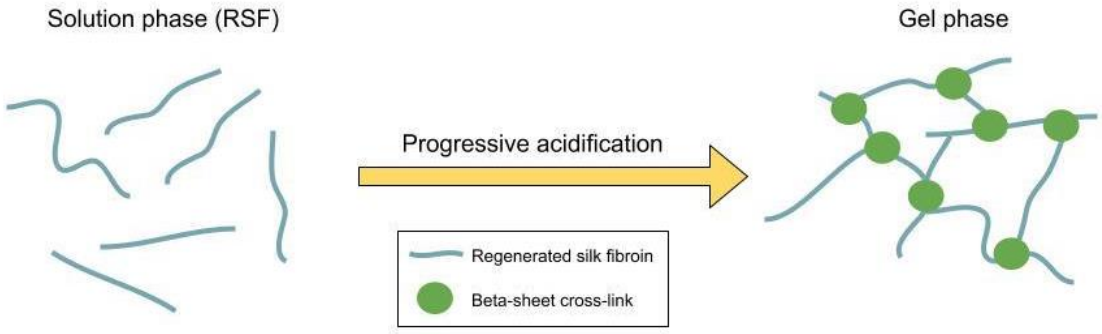

Fig. 9: Simplistic illustration of the self-assembly process of fibroins. Induced sol-to-gel transition triggers assembly of silk fibroin molecules via beta-sheet formation and physical entanglement.

When it comes to the study of the kinetics of protein self-assembly processes and gel formation, a variety of *in-situ/time-resolved* experiments can be employed. Gelation may thus be monitored using methods such as FTIR, fluorescence, NMR, and circular dichroism spectroscopy, alongside with scattering methods [59].

2.5. Thioflavin T: a ubiquitous marker of assembly and aggregation

Thioflavin T (ThT), likewise known as Basic Yellow 1 or CI 49005, is a widely used dye in aggregation studies of amyloids and proteins, as it fluoresces only when incorporated into rigid and confined microenvironments, such as fibrils and amyloid-like structures [60,61] (fig. 10, right). Structurally, ThT is comprised of a positively charged dimethylated benzothiazole ring connected to a dimethylamino benzyl ring via a single covalent C–C bond [60](fig. 10, left).

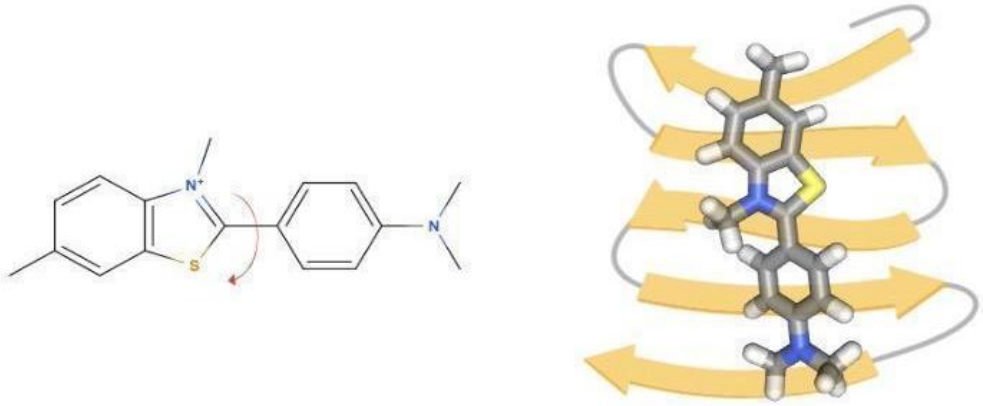

Fig. 10: Chemical structure of ThT highlighting its rotational C-C bond (left) and schematic representation of ThT "bound" to an unconfined environment, here represented by an antiparallel beta-sheet structure (right).

Quantum-yield calculations support the idea that this single sigma bond indeed allows viscosity-dependent torsional movement and relaxation of the two ThT rings relative to each other. [61–65] "Free ThT" has a non-fluorescent electronic decay from its S1 to S0 state in low viscosity environments. In confined and viscous solutions ("bound ThT to, i.e.: beta-sheet structures), an increase in fluorescence of ThT signal occurs, as internal free rotation of the rings is blocked due to steric hindrance. This results in high fluorescence quantum yield upon excitation. One can thus directly monitor the formation of beta-sheet structures in gels to understand their fibrillation mechanism and infer molecular events. ThT high selectivity and sensitivity allow direct quantification and characterization of the self-assembly kinetics across a variety of different physical systems.

Chapter 3: Materials and methods

3.1. Factorial design and optimization

In order to systematically study the interplay between different silk concentrations and its different self-assembly kinetics, a full factorial experiment consisting of 4 different silk concentrations (2,3,4,5 % wt/vol) and 5 different concentrations of ThT (0, 20, 50, 100, 300 µM ThT) was performed using Minitab (Minitab, LLC). After data collection, an optimization was run based on the best parameters for extrusion according to the proposed model (low drop in force and respective slope after initial push). Table 1 summarizes the randomized runs with factors used and their range.

Table 1: Full factorial table

Run order	Silk concentration (mg/ml)	Target ThT concentration (µM)
1	50	50
2	20	100
3	40	0
4	40	100
5	40	300
6	30	50
7	40	50
8	50	300
9	50	100
10	50	20
11	40	20
12	30	0
13	30	20
14	50	0
15	20	50
16	20	0
17	20	20
18	30	100
19	30	300
20	20	300

3.2. Materials

Bombyx mori degummed silk fibres were obtained from an online silk supplier (Wild Fibres, UK). Glucono-δ-lactone (GDL), Thioflavin T (ThT), Lithium Bromide (LiBr), and cellulose dialysis tube (12kDa MWCO) were purchased from Sigma - Aldrich.

3.3. Silk fibroin regeneration

Five grams of degummed silk fibres were dissolved in 50 mL 9 M LiBr solution for 30 minutes. Regeneration was performed in a controlled water heating bath, and the silk solution dissolved inside a glass container sealed with a plastic cover and at a constant inner temperature of 68 °C, in order to maximize

thermal conductivity and heat distribution, and prevent evaporation and hence changes in the silk/LiBr ratio. After dissolution, the solution was left to cool for 5 min, filtered through a piece of sterile 100% cotton gauze pads (here used to filter out debris from the regeneration process) and transferred to a cellulose dialysis tube (molecular weight cut-off of 12 kDa). The regenerated silk solution was dialyzed against 2 L buffer (10 mM sodium phosphate - NaP, pH7.2) for 3 days. The dialysis solution was changed twice a day, and it was considered finalized only after the designated days and provided the electroconductivity of the dialysis solution equaled the one of the buffer. After dialysis, the regenerated silk fibroin was transferred into a 50 mL falcon tube and centrifuged twice at 4500 rpm for 10 min at 20 °C to remove insoluble residues. The obtained solution was then stored in a refrigerator at 5 °C. The final concentration of the RSF solution was determined using a simple dry mass method.

3.4. Fabrication of biomimetic silk gels

In order to increase the data's statistical relevance of the samples from the factorial experiment, all the studies were performed from the same exact "sample batch". Hence, for each silk gel, as described in table 1, a main 5 mL sample solution was prepared in a 10 ml falcon tube by diluting the obtained RSF stock with 10 mM sodium phosphate buffer (NaP) down to its respective final concentration, and by diluting and adding the according ThT from a 10 mM initial stock. From this main sample solution, 4,5 mL were transferred and divided between three different 2,0 mL, each containing 1,5 mL of the main sample solution, being these tubes destined to different experiments (*tube 1* to turbidity, large-strain indentation and extrusion studies, *tube 2* to time-resolved fluorescence and ATR FT-IR). In order to promote the biomimetic self-assembly of the studied silks, GDL was used as a progressive and homogeneous acidification agent at 0.5% wt. Two additional 2 mL eppendorf tubes were used to pre-weight eppendorf tubes with GDL, and to each of these, the 1,5 mL samples from the main sample solution were added, and then gently mixed until the complete visual dissolution of the GDL. The solution from *tube 1* and GDL was immediately pipetted into a PMMA (Poly-methyl methacrylate) up to a final volume of 1,5 mL and the cuvettes sealed with plastic covers and parafilm to avoid any substantial drying of the gels during assembly. From the remaining volume, 300 µL were loaded into a 1 mL plastic syringe (Terumo) for extrusion studies. The GDL is added and mixed with the solution from tube 2 only after all the described tasks from tube 1 are completed, in order to maximize the amount of data collected from both time-resolved measurements. The solution from tube 2 is thus transferred and mixed in the tube containing GDL as described. 300 µL samples are then transferred to a 96 well plate (5 replicates were performed) and the plate covered with transparent film (Sigma Aldrich) in order to avoid any drying.

3.5. Extrusion studies

In order to assess the injectability and gel mechanical behaviour in pneumatic extrusion, an extrusion experiment was designed and performed using a setup consisting of a modified 3D-bioprinter (3D Cultures, Philadelphia, USA) with a flexible force sensor. A homemade 3D-printed adapter was installed on the top portion of the movable extruder in order to accommodate the sensor and the plunger of the syringe (fig. 11). Uniaxial extrusion was performed at a constant speed of 0,5 mm/s, as this specific speed falls within all the previously used speeds to study the syringeability of injectable systems.

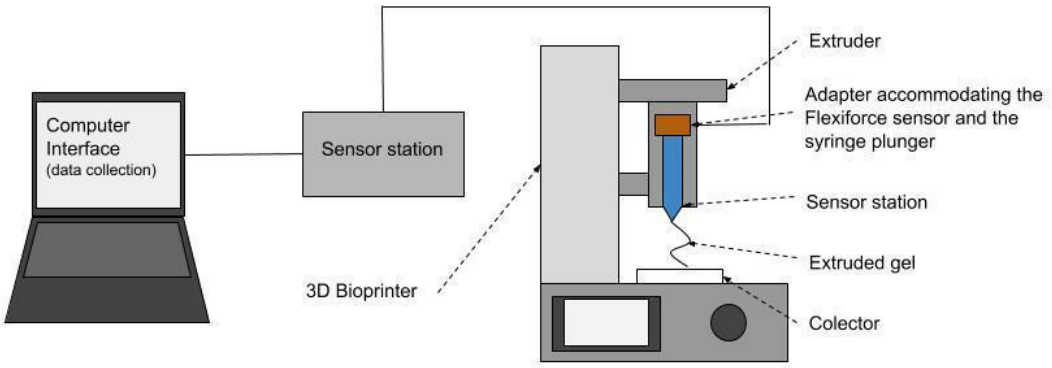

Fig. 11: Schematic representation of the extrusion setup.

3.6. Large-strain indentation

In order to study the intrinsic mechanical properties of the studied materials, large strain indentation in the silk gels was performed after a 19h gelation period in the same cuvettes, and without drying or transferring the sample in order to minimize disturbance. The indentation was performed using a V500c Mach-1 Mechanical Tester (Biomomentum Inc., Laval, QC) equipped 150g uniaxial load cell and a spherical indenter with a radius of 0,5 mm. Samples were indented at a rate of 0.1 mm/s to an indentation depth (*d*) of 5,40 mm, At this point, the gels were known to fail/puncture. At lower indentation depths, the intrinsic properties of the material can be accessed, and at deeper depths, spherical indenters give the same mechanical responses as their flat-punch counterparts, and most of the fracturing points of the studied gels were previously known to occur at these depths. No contact force parameters were set-up, in order to avoid any contact issues occurring from adhesion between the indenter and the samples. Young and shear modulus were calculated using the Mach-1 analyzer software, by fitting an elastic with spherical indentation model in the very beginning of the force-displacement curves.

3.7. Self-assembly and gelation kinetics

In order to understand if the self-assembly mechanism is determinant to the intrinsic mechanical properties and the extrusion profile of the studied soft gels, self-assembly studies on the kinetics of silk fibroin aggregation were performed using the biomimetic acidification approach. As it was of interest to both correlate different measurements and understand how the increase in gel network size is accompanied by physical network entanglement and stabilization, self-assembly kinetics were characterized by means of time-resolved fluorescence and UV-vis spectroscopy.

3.7.1. Fluorescence spectroscopy

For fluorescence studies, ThT was used to study the molecular mechanisms that encompass the biomimetic acidification of silks and was chosen due to its high specificity and selectivity to detect changes in microenvironment viscosity (see chapter 2). A 96-well plate was used and 5 repetitions of the 20 samples derived from the factorial design were performed (see section 3.4.) in a Cary Eclipse Spectrophotometer (Agilent Technologies). The excitation wavelength was set at 450 nm, with emission at 490, as this is the local maximum peak for fluorescence intensity of ThT [66–69].

Not only buffer subtraction, but correction for primary inner filter effect is critical to analyzing the data, especially at such high concentrations of ThT like the ones used. Thus, 5 repetitions of the same buffer were collected (10 mM NaP), while for primary inner filter correction, the absorbance spectra maximum of ThT was obtained during the turbidity measurements, and the correction factors, *W*, were calculated for each sample (see supplementary materials) using the following equation [70]:

$$W = \frac{1-10^{-A_{FL}}}{A_{FL}} \text{ (equation 1),}$$

where $A_{FL}$is defined as the maximum intensity peak in ThT turbidity at $time_{turbidity} = 0\,(min)$. Each of the points taken throughout the whole time-resolved measurement for each sample was corrected for the primary inner filter effect. Fluorescence intensity at a given time was divided by the respective correction factors for each sample, Wx , and the obtained intensity further subtracted with the averaged buffer signal. Both corrections and buffer subtraction was performed using an in-house Python script. After this, the same python script was used to fit all of the fluorescence traces with emission at 490 nm, in order to compute t_0,t_{lag}, and τ. To perform the non-linear curve fitting like in fluorescence, the scipy.optimize least square method was used, which automatically minimizes the sum of squares of the function (residuals) given as an argument. A simple biphasic model was used to fit the model, in order to account for the logarithmic-curve behaviour of the initial instances in the fluorescence traces. This initial log-like behaviour is associated with the origin of metastable oligomers in amyloid self-assembly [71]. The used fitting model was as follows:

$$y = a \times log\,(b + t) + y_0 + \frac{c}{1+e^{-k(t-t_0)}} \text{ (equation 2),}$$

3.7.2. Turbidity

In order to compare the same events in terms of light scattering, turbidity studies were performed by measuring the full absorbance spectra of the gels in 1,5 mL pathlength PMMA cuvettes (as already described in 3.4.) in a Cary 60 Spectrophotometer (Agilent Technologies). Silk turbidity was analyzed at 600 nm, due to low noise-to-signal ratio and to the fact that this wavelength is far away from the ThT turbidity peak. Other wavelengths, such as 360, 500, and 700 nm were also analyzed. The 360 nm wavelength showed complex non-sigmoidal profiles and the molecular events that encompass such curves still remain unclear. For that reason, it will not be analyzed in this report. 600 nm was chosen in detriment of 500 nm due to the reasons already specified, as 500 nm is still very much within the ThT curve-signal range, and at 700 nm, the signal starts to weaken. Buffer intensity subtractions were performed prior to the measurement by taking the baseline intensity of the 10mM NaP buffer. ThT changes in population are inferred using a centre of mass approach, considering the peak of ThT turbidity at 415 nm. Calculations for the centre of mass (or Barycentric mean) of ThT were computed using an in-house Matlab script (MATLAB, Mathworks Inc., USA) by applying the following model:

$$Centre\ of\ mass = \frac{\sum_i \lambda_i F_i}{F_i} \qquad \text{(equation 3).}$$

Each of the turbidity trace at 600 nm is fitted using the same in-house Matlab script, in order to extract their respective transition times (t_0, also known as half-times), lag phase times ($t_{lag}= 2\tau - t_0$), and steepness of the reaction ($\tau = \frac{1}{k}$). The following simple sigmoidal model was fitted:

$$y = y_0 + at + \frac{c+dt}{1+e^{k(t-t_0)}} \text{ (equation 4),}$$

where $(y_0 + at)$ and $(c+ dt)$ represent the turbidity intensity at the beginning and end of gelation, respectively, to correct for a non-flat start and end baseline.

3.8. Extrusion effects in gel secondary structures

In order to unravel the effects of the extrusion process in the gel secondary structure, the FTIR spectra of extruded and non-extruded gels were collected using a Thermo Scientific Nicolet 6700 infrared spectrometer equipped with a MiRacle ATR accessory and a diamond crystal (Pike Technologies). The center of mass approach was chosen as an evaluation method because it gives a simple, but fine and generalized measurement of the relative changes occurring in the Amide I region before and after extrusion. Specifically, the focus of the analysis is in Amide I area, as this is a very well-defined and characteristic fingerprint region of the infrared spectra of silks, and is present in the silk threads produced throughout a wide variety of different silkworm species [72]. Each sample spectrum consisted of 64 averaged scans at 4 cm^{-1} resolution at a fixed scan rate of 0,6329 $m \cdot s^{-1}$ in the range of 400-4000 cm^{-1}. Posteriorly, the centre of mass of the Amide I was calculated using the same method described in section 3.7.2 for the calculation of the center of mass of turbidity of ThT (equation 3).

3.9. pH measurement

In order to understand and characterize how the events accessed by spectroscopy correlate with the biomimetic progressive acidification method used, a pH measurement was performed in parallel to spectroscopy in a time-resolved manner and for all samples without ThT. The process was monitored using a Hamilton HI2210 pH-meter hooked and recorded to a LabQuest® Mini sensor (Vernier Software & Technology, USA), by collecting a reading every 5 minutes for 18 hours at 20°C (room temperature).

Chapter 4: Results

Can we reach a relevant artificial extrusion of silks by mimicking the way silk is processed and spun?

To provide an answer to that, biomimetic acidification is used, combined with the scanning and optimization of the best properties for extrusion at common injection speeds (0,5 mm/s). In order to characterize the impact of the biomimetic acidification in the extrusion properties of gels, a combination of spectroscopy and mechanical techniques were used. Due to the nature of the obtained data, we will first need to understand and define the visual correlation between a damaged and undamaged gel, and how does that observation correlates to their secondary structures.

4.1. Definition of damaged and undamaged gels

In order to understand the definition of a damaged matrix, and the impacts of the extrusion process in gel nature, we studied gel secondary structure using infrared spectroscopy. First and foremost, the extrusion process establishes the emergence of two very different gel populations. In one population, we have a group of gels that can be extruded without damage, and in the other, we have a population of gels completely damaged after extrusion at common injection rate (fig.12).

Figure 12 (top right and left) illustrates an example of what we defined as a damaged gel (3% wt. 100 μM ThT) and undamaged gel (4% wt. 20 μM ThT) after extrusion.

In a damaged gel, there is evident loss of intensity in the Amide I spectra when compared to a non-damaged one.

The centre of mass of the Amide I is hence used here to pick up and quantify this correlation between a visually damaged gel and its secondary structure.

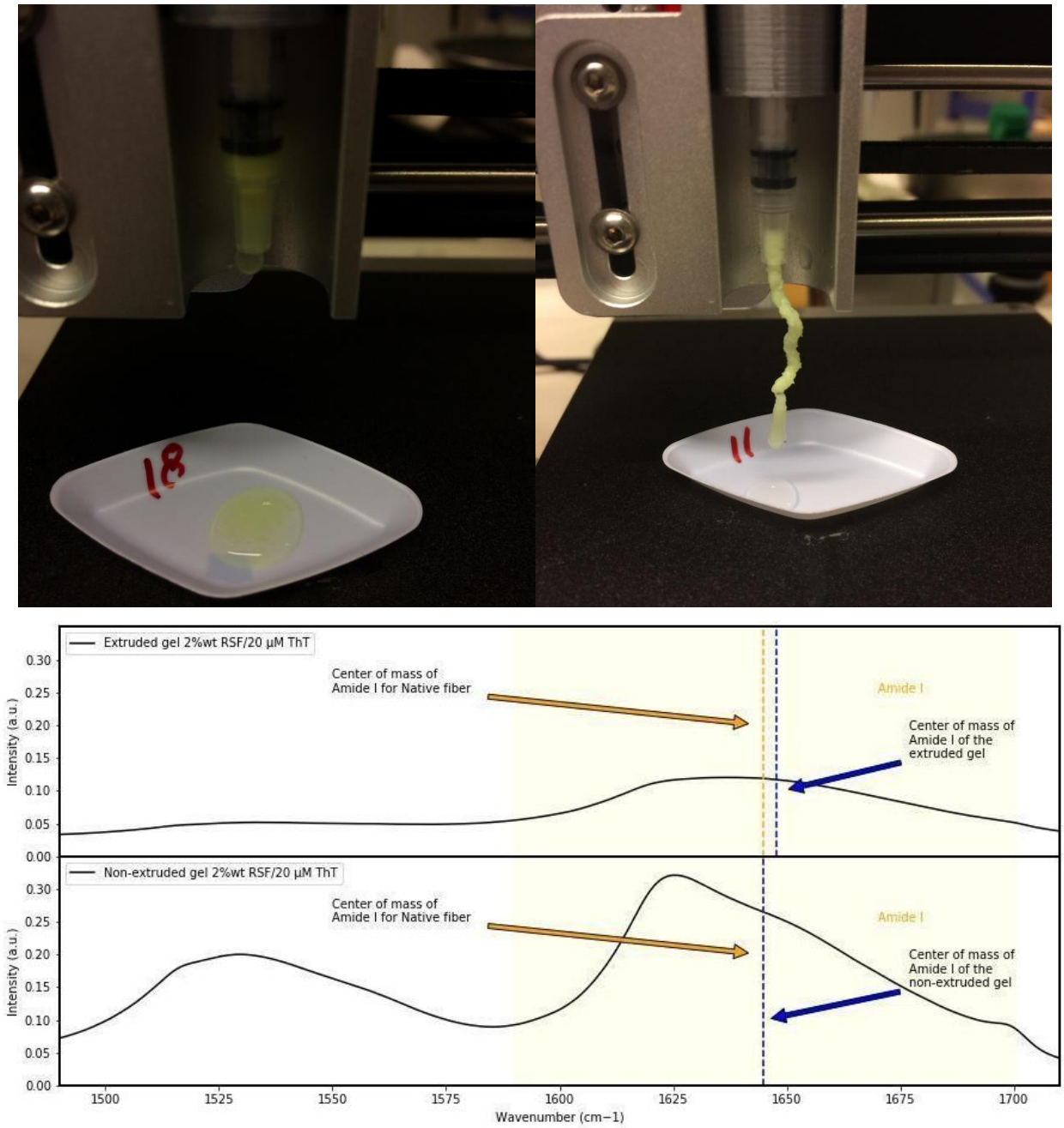

Fig. 12: (Top) Example of a damaged (left) and non-damaged (right) gel after extrusion at 0,5 mm/s. It is clear by the evidence the degree of destruction of a concentration gel comprises their viability as injectable matrices. (Bottom) Full infrared spectra obtained from Fourier Transform-Infrared spectroscopy data with an ATR setup elucidating the changes in spectra intensity of an exemplar of a gel that was damaged during the extrusion process. The differences captured via infrared spectroscopy of the same gel after and before being extruded are evident. The dashed lines (--) represent the corresponding wavenumber (cm^{-1}) for the centre of mass of the Amide I of the studied gel (blue) before and after being extruded. The centre of mass of a native *Bombyx mori* spun fibre (orange) is shown for comparison purposes. The yellow area represents the Amide I region.

4.2. Structures of the extruded and non-extruded gels – ATR FT-IR

Surprisingly, gels before extrusion have minimal to negligible changes in their centre of mass of the Amide I, and they are incredibly close to the center of mass of a native spun *B. mori* fibre (fig. 13 and 14). The closeness and relevance of the biomimetic acidification are apparent, as the gels' secondary structures are close to the ones seen in a native spun fibre.

There is a definite shift in the centre of mass of the Amide I in gels that were damaged by the extrusion process, and relatively minimal to no changes in the centre of mass of gels that were undamaged. These observations hint towards the existence of a critical silk concentration (between 3 and 4% wt. silk) that separates and defines when a gel is damaged or not during extrusion. Extruded gels at and above 4% wt. silk concentration unanimously reveals no substantial changes in their centre of mass Amide I compared to their non-extruded counterparts. This thus leads to the conclusion that, at these silk concentrations, silk gels can be extruded without the total disruption of their network (see discussion).

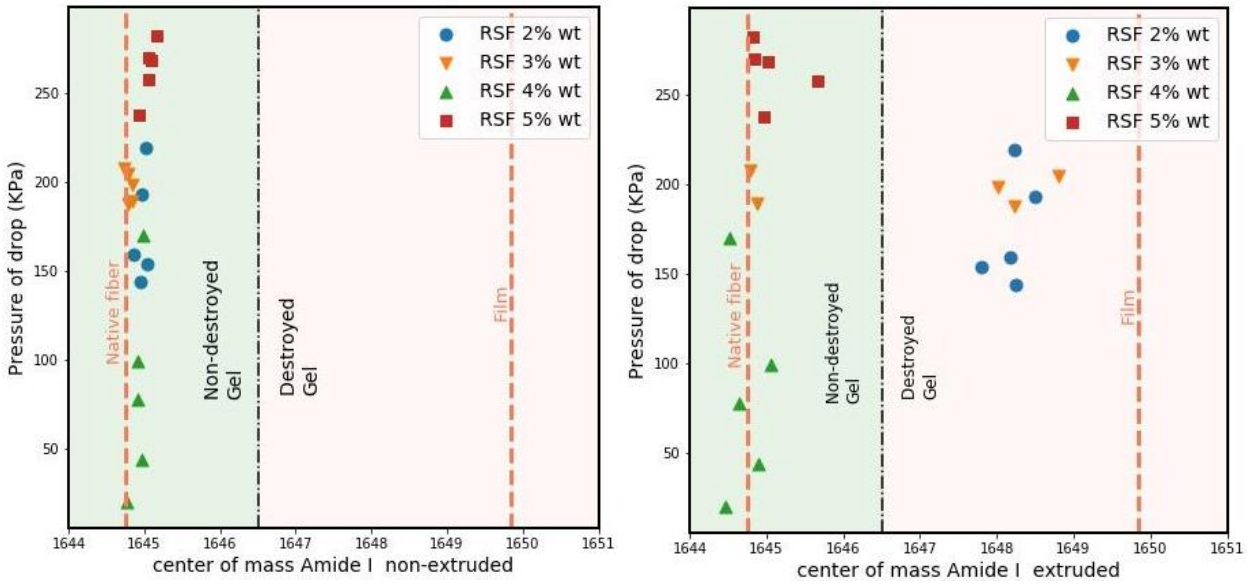

Fig. 13: Centre of mass of the Amide I accessed from Infrared spectroscopy of non-extruded (left) extruded gels (rigt) as a function of the registered pressure in drop upon after initial displacement extrusion. The dashed lines (--) represent the corresponding wavenumber (cm^{-1}) for the centre of mass of the Amide I for both a film and native *Bombyx mori* spun fibre and are shown for comparison purposes. The red and green areas are arbitrary areas shown for representation of the group of gels that were damaged and non-damaged upon extrusion. The dashed lines that separates these areas does not correspond to any specific wavenumber and is here only for representation purposes.

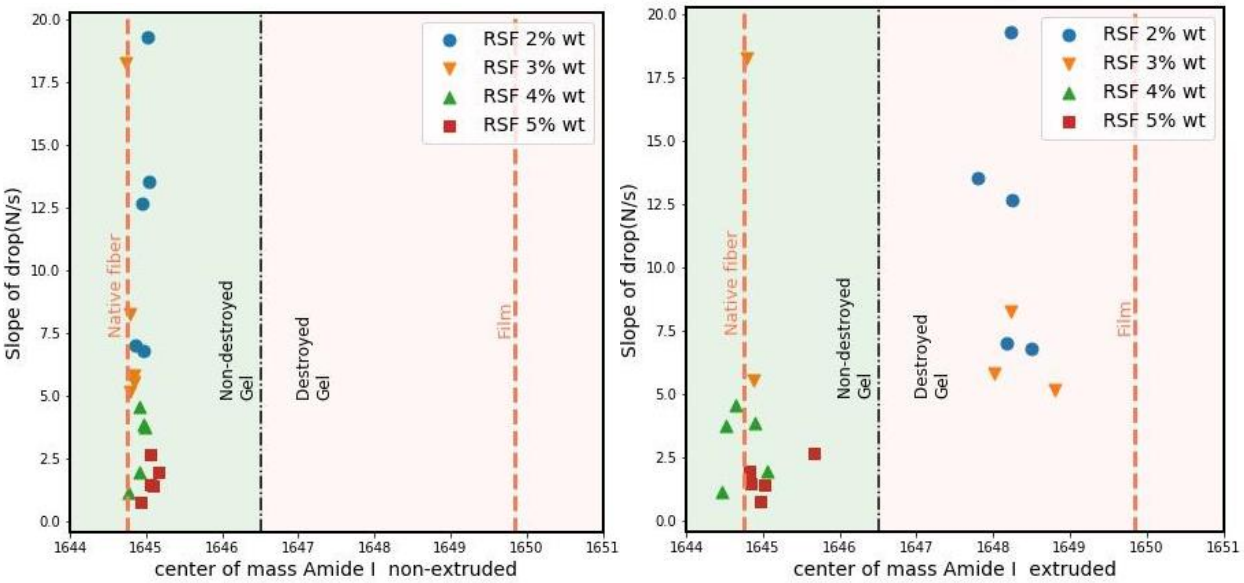

Fig. 14: Centre of mass of the Amide I accessed from Infrared spectroscopy of non-extruded (left) extruded gels (right) as a function of the registered slope of the after initial displacement upon extrusion. The dashed lines (--) represent the corresponding wavenumber (cm^{-1}) for the centre of mass of the Amide I for both a film and native *Bombyx mori* spun fibre and are shown for comparison purposes. The red and green areas are arbitrary areas shown for representation of the group of gels that were damaged and non-damaged upon extrusion. The dashed lines that separates these areas does not correspond to any specific wavenumber and is here only for representation purposes.

Furthermore, a critical set of conditions associated with the 4% wt. silk concentration starts to pop up. At these concentrations, the lowest values for drop pressure and respective slope were recorded. As mentioned, this fibre is not damaged. According to part of the hypothesis, a relevant bio-inspired artificial extrusion can be achieved by minimizing a set of parameters, such as the drop and slope of the drop after initial gel displacement. Optimization results for the full factorial experiment do start to reveal around a 4% wt. silk concentration (see discussion)

4.3. Silk extrusion and correlation to the mechanical properties of pre-extruded gels

By rapidly looking at figures 15, 16, and 17, one easily understands that the intrinsic properties of the gels demonstrate their biological relevance. Apart from the highest studied silk concentration (5% wt.), all silk gels fall well within the biologically-relevant extrusion domain, and their Young modulus is always lower than the maximum recorded pressure in hard-bodied insects – 40 KPa. Interestingly, lower concentrations show intrinsic properties equal to the haemocoelic pressure limit in *B mori*. We know already from the FT-IR analysis that these gels, although in close magnitude to the physiological properties of *B. mori* silk glands, do not generate, nor display the characteristics of a good extrusion. As of fact, we know from the correlation between the centre of mass Amide I and the visual state of the gels, that 2 and 3% wt. silk concentration cannot even be considered to be gels after extrusion at common injection speed. This further

confirms the robustness of both utilizing a model for a good extrusion in combination with a biological understanding of the animals that naturally spin silk.

In all the analyzed parameters (initial push, drop and slope of drop), there always seem to be a displacement of the gels that do resist extrusion (2 and 3% wt.) and a linear correlation between the mechanical properties and the extrusion parameters of both the 4 and 5% wt. silk concentration.

The full factorial and ANOVA analysis do point out a strong linear correlation between the extrusion properties and the mechanical properties of the gels. There is thus a direct relationship between the concentration of the silk gels formed under biomimetic acidification and the extrusion properties of the gels extruded at common injection speed.

Furthermore, 4% wt. silk concentration seems to be the local minimum in this linear relationship where the extrusion parameters are minimized (fig. 15, 16, and 17). At the same time, this concentration seems to be at a local minimum where extrusion with biological relevance is achieved. The interception of the optimal regions provided by the two models seems to define a relevant bio-inspired artificial extrusion at 4% wt. silk concentration ("*sweet spot*" concentration).

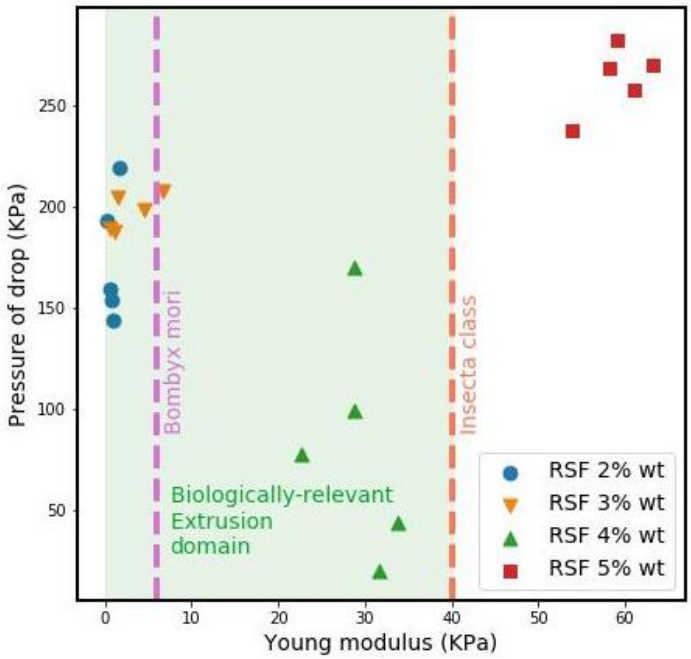

Fig 15: Pressure of the drop after the initial push as a function of the intrinsic mechanical properties (Young modulus) of the studied gels. The dashed lines (--) represent the corresponding maximum internal recorded pressure in the *Insecta* class (40 KPa) (red) and the haemocoelic rupture pressure of final instar *Bombyx mori* entering pupation (5,88 KPa) (yellow). The biologically-relevant extrusion domain (green area) is defined as the range where artificial extrusion as biological relevance.

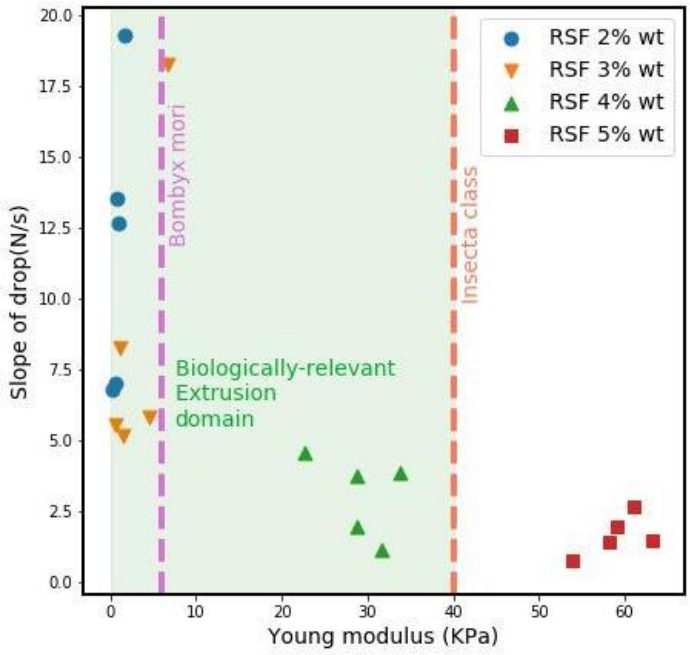

Fig 16: Slope of the drop after the initial push (bottom) as a function of the intrinsic mechanical properties (Young modulus) of the studied gels. The dashed lines (--) represent the corresponding maximum internal recorded pressure in the *Insecta* class (40 KPa) (red) and the haemocoelic rupture pressure of final instar *B. mori* entering pupation (5,88 KPa) (yellow). The biologically-relevant extrusion domain (green area) is defined as the range where artificial extrusion as biological relevance.

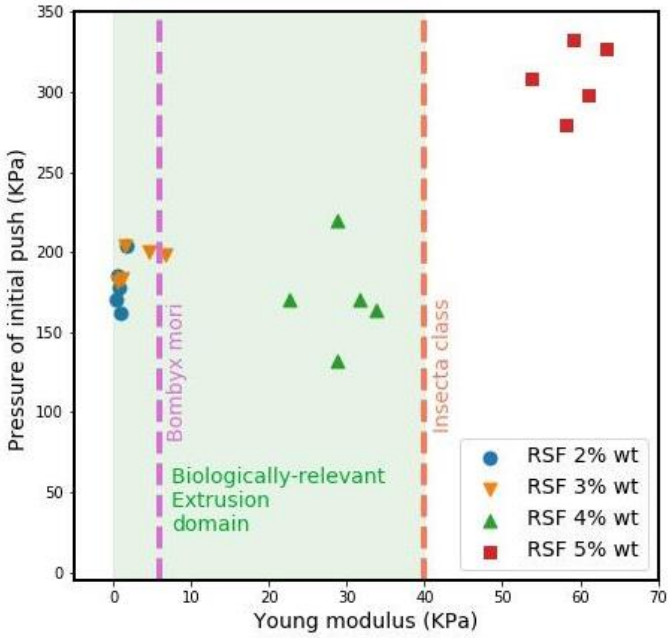

Fig 17: Pressure requirements for initial push as a function of the intrinsic mechanical properties (Young modulus) of the studied gels. The dashed lines (--) represent the corresponding maximum internal recorded pressure in the *Insecta* class (40 KPa) (red) and the haemocoelic rupture pressure of final instar *Bombyx mori* entering pupation (5,88 KPa) (yellow). The biologically-relevant extrusion domain (green area) is defined as the range where artificial extrusion as biological relevance.

4.3. Self-assembly of the pre-extruded gels

Both silk and ThT concentrations seem to affect the transition times (half-times) as studied by fluorescence (fig. 19). ANOVA and full factorial results support the statically relevance of that observation, with a stronger effect of ThT (see supplementary materials). Both entities seem to also have a statistically relevant effect in modulating the lag phase times as studied by turbidity (fig. 20). However, in this case, the influence of silk concentration is more pronounced, as it is demonstrated by its high F-value (see supplementary materials)

To better understand the effects of progressive acidification, the different spectroscopy data was overlaid for all of the 4% wt. silk fibroin gels containing ThT (fig. 20). One can note the aptness of the used gelation approach in recreating a truly relevant biomimetic acidification. The first transition in turbidity (first sharp increase in turbidity intensity peak) happens at pH 3,75. This is rather expected, as silk fibroin proteins are generally reported to have their isoelectric point between 3,6 and 5,2 pH [73]. The sharp transition in the ThT signal seems to always occur when no more light is being scattered, leading to believe that structural growth and beta-sheet formation do not correspond to the same event.

Likewise, worthy to note is the fact that there seems to be a universally clear hypsochromic (blue) shift of the centre of mass of ThT, which is associated with the first transition in turbidity, and always followed by a strong bathochromic (red) shift. Additionally, the presence of a defining slope in ThT centre of mass during the initial stages of gelation, and the fact that this slope seems to decay as one goes up in ThT concentration points out to the presence of some molecular events occurring during the lag phase of the self-assembly process. This could be due to the increase in the ThT-to-silk ratio, which hides the relative signal contribution produced from this slowly shifting ThT population, whose behaviour seems to be well-depicted at 20 μM ThT.

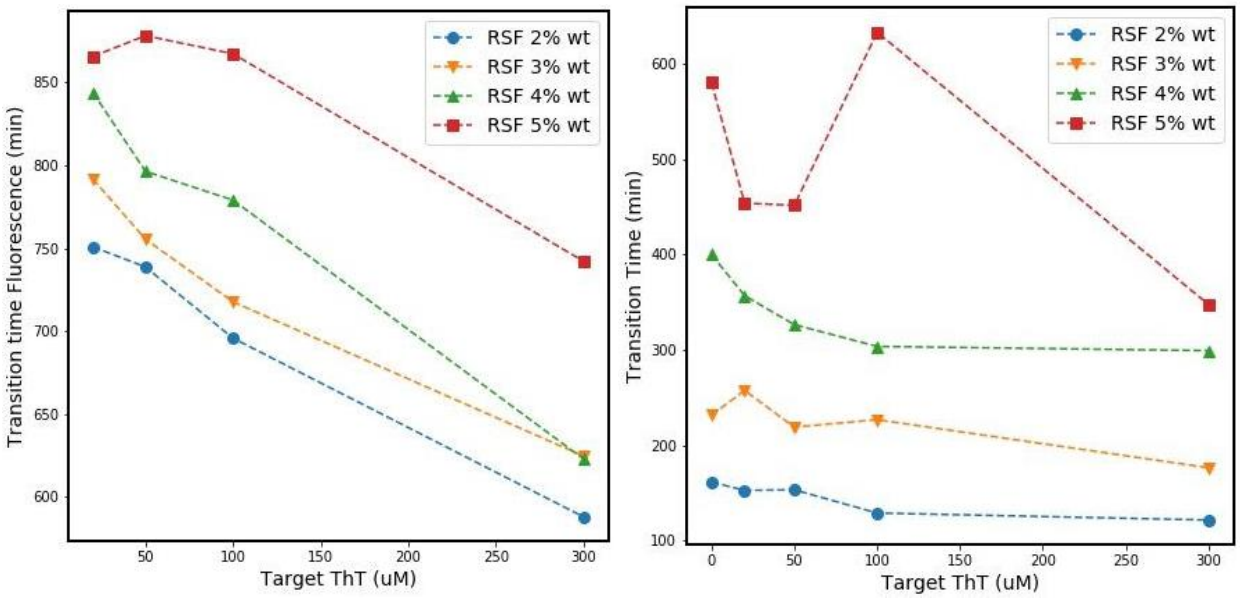

Fig 19: Transition times (left) and lag phases (right) of the various samples, by means of fluorescence and turbidity, respectively.

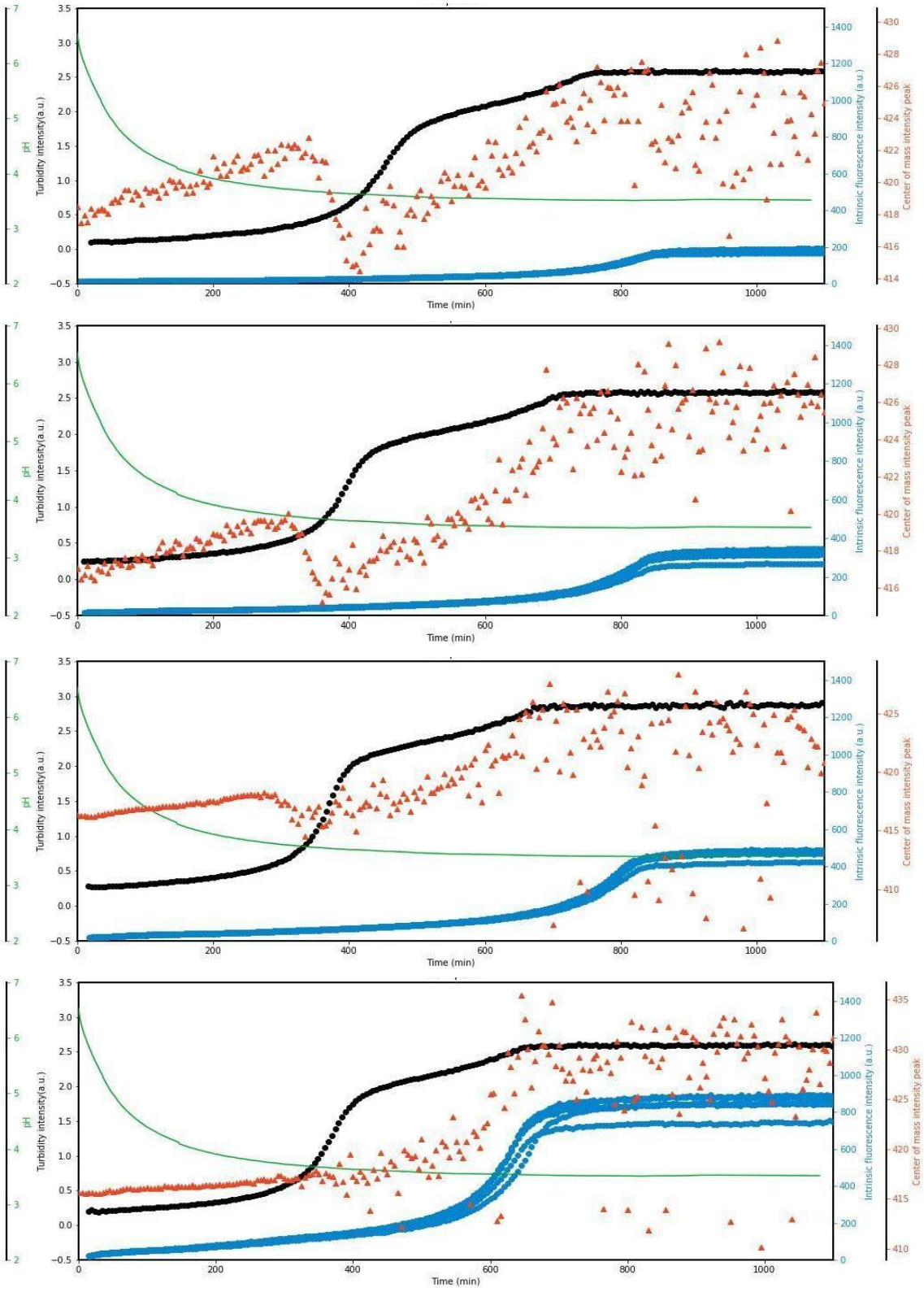

Fig. 20 Self-assembly kinetic plots of the 4wt% silk concentration at 0, 20, 50, 100, and 300 μM ThT (respectively, from top to bottom). Each plot is overlaid with its own respective sample of pH (green), centre of mass of ThT (red), fluorescence intensity (blue), and turbidity measurements (black) over time.

Chapter 5: Discussion

Silks are the refined product of evolution towards a cost-efficient spinning. [74] Within the scarce number of silk injectable gels today [1–7,9,44], all lack a true biomimetic nature. We then asked if, by mimicking the natural way silks are processed and spun by the animal, and by optimizing gels for their best extrusion properties, we could obtain a biologically relevant artificial extrusion of silks.

Apart from 5% wt. all the intrinsic mechanical properties of the gels are shown to be well within the biological relevance. The rationale was that, in order to achieve an artificial extrusion with biological relevance, these gel mechanical properties would need to be within the physiological capacity of the structures associated with silk spinning. The relevance is inferred by rationalizing that, provided silk-spinning was an extrusion-dominated process, the natural silk spinners would still be able to extrude silk without compromising internal their internal structures. This is true for all the biomimetic gels (apart from 5% wt.), and relevant to all species in the *Insecta class*. The use of biomimetic acidification and extrusion at common injection speeds, coupled with the use of a mechanistic optimal injectable model, have proven that a biologically relevant artificial extrusion of silks is indeed achievable.

Additionally to the appearance of extrusion within the biological spinning domain, the emergence of a critical point in fibroin concentration, where injectability is allowed, is also reported. At this *sweet spot*, the relatively low-pressure requirements allow the displacement of a gel without compromising its network (fig 15, 16, and 17). 4% wt. silk concentration does pop up as an optimal concentration from the factorial analysis, where the emergence of bio-inspired artificial injectability occurs. It seems to exist something intrinsically special about this silk concentration, as 5% wt. gels do not evidence as characteristics of a good extruded system. One does understand that there is a very narrow boundary around 4% wt. silk concentration where the gel is not too tough to have bad extrusion properties (as at 5% wt.), but that is also not too soft to lead to network disruption upon extrusion (2 and 3%. wt.) Hence, there seems to be a very fine and critical set of conditions in silk gels (*silk sweet's spot*), where silks display biologically relevant artificial extrusion properties with a clear injectability component.

Only the silk concentration and the progressive acidification seem to play a role in the emergence of a true biologically relevant extrusion. Although modifying the kinetics of self-assembly, the statistical relevance of the influence of ThT seems to fade at a macroscopic scale (mechanics and extrusion). It is then concluded that ThT is only acting as a reporter.

Since ThT is a direct reporter of beta-sheet formation [60,75], one can thus assume that a major network entanglement and polymeric physical entanglement only occur at the end-stage points of gelation, when there is no more growth in the size of the gel structures. Intrinsic mechanical properties are the reflection degree of cross-linkage. Silk concentration determines cross-linkage density, which therefore translates to the emergence of biologically relevant properties in extrusion.

The dimerization and stabilization of the N-terminal domain in silks are associated with pH gradient and is essential for spinning. [30,31,76,77,30,31] Since progressive biomimetic acidification is employed, one could then ask if this was also a key to achieve the relevancy of the extrusion process. The spectral shifts in the ThT center of mass could hold that answer. Nonetheless, a connection between the extrusion properties and both

the spectral shifts in the ThT center of mass, or even if they associated with a possible dimerization, as not yet been drawn.

It has then been demonstrated that a biologically-relevant artificial extrusion of silks can be achieved, when a truly biomimetic approach is combined with optimization of the mechanics that encompass extrusion. Processing gels like animals do, and optimizing for their extrusion properties, has revealed the emergence of a critical silk concentration, coined here *silk´s sweet spot*. At these conditions, both a biological relevant artificial extrusion and injectability are achievable, according to the proposed definition of an ideal extrusion process.

Conclusion

The presented data demonstrates that, even though silk spinning is a pultrusion-dominated process, one can achieve a biologically-relevant extrusion of silks that falls within the physiological capacities of the organisms that naturally spin silk. Furthermore, it is reported the existence of a specific concentration of silk ("*silk's sweet spot*"), where extruded gels reveal characteristics of an ideal injectable matrix, as defined according to the presented extrusion model. The formulation and optimization of injectable silk (hydro)gels for biomedical applications is rather irrelevant unless they are targeted to be formulated at this specific *sweet spot* concentration.

References

1. Hu, J. *et al.* Injectable silk fibroin/polyurethane composite hydrogel for nucleus pulposus replacement. *J. Mater. Sci. Mater. Med.* **23**, 711–722 (2012).
2. Gong, Z., Yang, Y., Ren, Q., Chen, X. & Shao, Z. Injectable thixotropic hydrogel comprising regenerated silk fibroin and hydroxypropylcellulose. *Soft Matter* vol. 8 2875 (2012).
3. Yucel, T., Cebe, P. & Kaplan, D. L. Vortex-induced injectable silk fibroin hydrogels. *Biophys. J.* **97**, 2044–2050 (2009).
4. Meng, L. *et al.* Autonomic Self-Healing Silk Fibroin Injectable Hydrogels Formed via Surfactant-Free Hydrophobic Association. *ACS Appl. Mater. Interfaces* (2019) doi:10.1021/acsami.9b19415.
5. Wang, X. *et al.* Injectable silk-polyethylene glycol hydrogels. *Acta Biomater.* **12**, 51–61 (2015).
6. Chouhan, D., Lohe, T.-U., Samudrala, P. K. & Mandal, B. B. In Situ Forming Injectable Silk Fibroin Hydrogel Promotes Skin Regeneration in Full Thickness Burn Wounds. *Adv. Healthc. Mater.* **7**, e1801092 (2018).
7. Partlow, B. P. *et al.* Highly tunable elastomeric silk biomaterials. *Adv. Funct. Mater.* **24**, 4615–4624 (2014).
8. Injectable silk hydrogel for treating degenerated disc. *Nature India* (2015) doi:10.1038/nindia.2015.63.
9. Wu, H. *et al.* Injectable and pH-Responsive Silk Nanofibre Hydrogels for Sustained Anticancer Drug Delivery. *ACS Appl. Mater. Interfaces* **8**, 17118–17126 (2016).
10. Palomino-Durand, C. *et al.* Influence of the

SolubleInsoluble Ratios of Cyclodextrins Polymers on the Viscoelastic Properties of Injectable ChitosanBased Hydrogels for Biomedical Application. *Polymers* vol. 11 214 (2019).

11. You, Y., Xie, Y. & Jiang, Z. Injectable and biocompatible chitosan-alginic acid hydrogels. *Biomed. Mater.* **14**, 025010 (2019).
12. Thi, P. L., Le Thi, P., Lee, Y., Nguyen, D. H. & Park, K. D. In situ forming gelatin hydrogels by dual-enzymatic cross-linking for enhanced tissue adhesiveness. *Journal of Materials Chemistry B* vol. 5 757–764 (2017).
13. Cao, W. *et al.* The preparation and biocompatible evaluation of injectable dual crosslinking hyaluronic acid hydrogels as cytoprotective agents. *Journal of Materials Chemistry B* vol. 7 4413–4423 (2019).
14. Ji, D.-Y., Kuo, T.-F., Wu, H.-D., Yang, J.-C. & Lee, S.-Y. A novel injectable chitosan/polyglutamate polyelectrolyte complex hydrogel with hydroxyapatite for soft-tissue augmentation. *Carbohydrate Polymers* vol. 89 1123–1130 (2012).
15. Seong, Y.-J. *et al.* Hyaluronic Acid-Based Hybrid Hydrogel Microspheres with Enhanced Structural Stability and High Injectability. *ACS Omega* **4**, 13834–13844 (2019).
16. Wang, Q., Sun, C., Xu, B., Tu, J. & Shen, Y. Synthesis, physicochemical properties and ocular pharmacokinetics of thermosensitive in situ hydrogels for ganciclovir in cytomegalovirus retinitis treatment. *Drug Deliv.* **25**, 59–69 (2018).
17. Su, D. *et al.* Enhancing Mechanical Properties of Silk Fibroin Hydrogel through Restricting the Growth of β-Sheet Domains. *ACS Appl. Mater. Interfaces* **9**, 17489–17498 (2017).
18. Moreau, R. Variations de la pression interne au cours de l'émergence et de l'expansion des ailes chez Bombyx mori et Pieris brassicae. *Journal of Insect Physiology* vol. 20 1475–1480 (1974).
19. Harding, S. M. M. M. J. P. & S. M. Manton Mrs J. P. Harding. The evolution of arthropodan locomotory mechanisms. Part 9. Functional requirements and body design in Symphyla and Pauropoda and the relationships between Myriapoda and pterygote Insects. *Journal of the Linnean Society of London, Zoology* vol. 46 103–141 (1966).
20. Manton, S. M. The evolution of arthropodan locomotory mechanisms. Part 8. Functional requirements and body design in Chilopoda, together with a comparative account of their skeleto-muscular systems and an Appendix on a comparison between burrowing forces of annelids an. *Journal of the Linnean Society of London, Zoology* vol. 45 251–484 (1965).
21. Manton, S. M. The evolution of arthropodan locomotory mechanisms. *Zoological Journal of the Linnean Society* vol. 51 203–400 (1972).
22. Andersson, M., Johansson, J. & Rising, A. Silk Spinning in Silkworms and Spiders. *Int. J. Mol. Sci.* **17**, (2016).
23. Vollrath, F. & Knight, D. P. Liquid crystalline spinning of spider silk. *Nature* vol. 410 541–548 (2001).

24. Foelix, R. *Biology of Spiders*. (Oxford University Press, 2010).
25. Vollrath, F., Porter, D. & Dicko, C. The structure of silk. *Handbook of Textile Fibre Structure* 146–198 (2009) doi:10.1533/9781845697310.1.146.
26. Vollrath, F. Spider Webs and Silks. *Scientific American* vol. 266 70–76 (1992).
27. Dicko, C., Vollrath, F. & Kenney, J. M. Spider silk protein refolding is controlled by changing pH. *Biomacromolecules* **5**, 704–710 (2004).
28. Dicko, C., Kenney, J. M., Knight, D. & Vollrath, F. Transition to a beta-sheet-rich structure in spidroin in vitro: the effects of pH and cations. *Biochemistry* **43**, 14080–14087 (2004).
29. Domigan, L. J. *et al*. Carbonic anhydrase generates a pH gradient in Bombyx mori silk glands. *Insect Biochemistry and Molecular Biology* vol. 65 100–106 (2015).
30. He, Y.-X. *et al.* N-Terminal domain of Bombyx mori fibroin mediates the assembly of silk in response to pH decrease. *J. Mol. Biol.* **418**, 197–207 (2012).
31. Landreh, M. *et al.* A pH-dependent dimer lock in spider silk protein. *J. Mol. Biol.* **404**, 328–336 (2010).
32. Guan, J., Porter, D. & Vollrath, F. Thermally Induced Changes in Dynamic Mechanical Properties of Native Silks. *Biomacromolecules* vol. 14 930–937 (2013).
33. Kuang, D. *et al.* Highly elastomeric photocurable silk hydrogels. *Int. J. Biol. Macromol.* **134**, 838–845 (2019).
34. Wang, X. *et al.* Bioactive Silk Hydrogels with Tunable Mechanical Properties. *J. Mater. Chem. B Mater. Biol. Med.* **6**, 2739–2746 (2018).
35. Choi, J., McGill, M., Raia, N. R., Hasturk, O. & Kaplan, D. L. Silk Hydrogels Crosslinked by the Fenton Reaction. *Adv. Healthc. Mater.* **8**, e1900644 (2019).
36. Kim, M. H. & Park, W. H. Chemically cross-linked silk fibroin hydrogel with enhanced elastic properties, biodegradability, and biocompatibility. *Int. J. Nanomedicine* **11**, 2967–2978 (2016).
37. Lin, Y. *et al.* Tuning Chemical and Physical Cross-Links in Silk Electrogels for Morphological Analysis and Mechanical Reinforcement. *Biomacromolecules* vol. 14 2629–2635 (2013).
38. Floren, M. L., Spilimbergo, S., Motta, A. & Migliaresi, C. Carbon dioxide induced silk protein gelation for biomedical applications. *Biomacromolecules* **13**, 2060–2072 (2012).
39. Wang, X., Kluge, J. A., Leisk, G. G. & Kaplan, D. L. Sonication-induced gelation of silk fibroin for cell encapsulation. *Biomaterials* **29**, 1054–1064 (2008).
40. Li, X. *et al.* Soft freezing-induced self-assembly of silk fibroin for tunable gelation. *Int. J. Biol. Macromol.* **117**, 691–695 (2018).
41. Lu, Q. *et al.* Silk fibroin electrogelation mechanisms. *Acta Biomater.* **7**, 2394–2400 (2011).
42. Gong, Z., Yang, Y., Huang, L., Chen, X. & Shao, Z. Formation kinetics and fractal characteristics of regenerated silk fibroin alcogel developed from nanofibrillar network. *Soft Matter* vol. 6 1217 (2010).
43. Kim, U.-J. *et al.* Structure and Properties of Silk Hydrogels. *Biomacromolecules* vol. 5 786–792

(2004).

44. Injectable silk hydrogel for treating degenerated disc. *Nature India* (2015) doi:10.1038/nindia.2015.63.
45. Das, S. *et al.* Bioprintable, cell-laden silk fibroin-gelatin hydrogel supporting multilineage differentiation of stem cells for fabrication of three-dimensional tissue constructs. *Acta Biomater.* **11**, 233–246 (2015).
46. Ming, J., Bie, S., Jiang, Z., Wang, P. & Zuo, B. Novel hydroxyapatite nanorods crystal growth in silk fibroin/sodium alginate nanofibre hydrogel. *Materials Letters* vol. 126 169–173 (2014).
47. Silva, R. *et al.* Soft-matrices based on silk fibroin and alginate for tissue engineering. *Int. J. Biol. Macromol.* **93**, 1420–1431 (2016).
48. Aramwit, P., Kanokpanont, S., De-Eknamkul, W. & Srichana, T. Monitoring of inflammatory mediators induced by silk sericin. *J. Biosci. Bioeng.* **107**, 556–561 (2009).
49. Nultsch, K. *et al.* Effects of Silk Degumming Process on Physicochemical, Tensile, and Optical Properties of Regenerated Silk Fibroin. *Macromolecular Materials and Engineering* vol. 303 1800408 (2018).
50. Nam, J. & Park, Y. H. Morphology of regenerated silk fibroin: Effects of freezing temperature, alcohol addition, and molecular weight. *Journal of Applied Polymer Science* vol. 81 3008–3021 (2001).
51. Wang, Q., Chen, Q., Yang, Y. & Shao, Z. Effect of various dissolution systems on the molecular weight of regenerated silk fibroin. *Biomacromolecules* **14**, 285–289 (2013).
52. Xie, F. & Liang, H. Effect of Concentration on Structure and Properties of Concentrated Regenerated Silk Fibroin Solution. *Advanced Materials Research* vols 311-313 1653–1656 (2011).
53. Greving, I., Dicko, C., Terry, A., Callow, P. & Vollrath, F. Small angle neutron scattering of native and reconstituted silk fibroin. *Soft Matter* vol. 6 4389 (2010).
54. Dicko, C., Kenney, J. M. & Vollrath, F. β-Silks: Enhancing and Controlling Aggregation. *Advances in Protein Chemistry* 17–53 (2006) doi:10.1016/s0065-3233(06)73002-9.
55. Martin, F. *et al.* Effect of oxidoreduction potential and of gas bubbling on rheological properties and microstructure of acid skim milk gels acidified with glucono-delta-lactone. *J. Dairy Sci.* **92**, 5898–5906 (2009).
56. Del Giudice, A., Dicko, C., Galantini, L. & Pavel, N. V. Time-Dependent pH Scanning of the Acid-Induced Unfolding of Human Serum Albumin Reveals Stabilization of the Native Form by Palmitic Acid Binding. *J. Phys. Chem. B* **121**, 4388–4399 (2017).
57. The physics of protein self-assembly. *Curr. Opin. Colloid Interface Sci.* **22**, 73–79 (2016).
58. Seroski, D. T. & Hudalla, G. A. Self-Assembled Peptide and Protein Nanofibres for Biomedical Applications. *Biomedical Applications of Functionalized Nanomaterials* 569–598 (2018) doi:10.1016/b978-0-323-50878-0.00019-7.
59. Arosio, P., Knowles, T. P. J. & Linse, S. On the lag phase in amyloid fibril formation. *Physical Chemistry*

Chemical Physics vol. 17 7606–7618 (2015).

60. Gade Malmos, K. *et al.* ThT 101: a primer on the use of thioflavin T to investigate amyloid formation. *Amyloid* **24**, 1–16 (2017).
61. Stsiapura, V. I., Maskevich, A. A., Kuzmitsky, V. A., Turoverov, K. K. & Kuznetsova, I. M. Computational Study of Thioflavin T Torsional Relaxation in the Excited State. *The Journal of Physical Chemistry A* vol. 111 4829–4835 (2007).
62. Stsiapura, V. I. *et al.* Thioflavin T as a molecular rotor: fluorescent properties of thioflavin T in solvents with different viscosity. *J. Phys. Chem. B* **112**, 15893–15902 (2008).
63. Maskevich, A. A. *et al.* Spectral Properties of Thioflavin T in Solvents with Different Dielectric Properties and in a Fibril-Incorporated Form. *Journal of Proteome Research* vol. 6 1392–1401 (2007).
64. Voropai, E. S. *et al.* Spectral Properties of Thioflavin T and Its Complexes with Amyloid Fibrils. *Journal of Applied Spectroscopy* vol. 70 868–874 (2003).
65. Stsiapura, V. I., Maskevich, A. A., Tikhomirov, S. A. & Buganov, O. V. Charge transfer process determines ultrafast excited state deactivation of thioflavin T in low-viscosity solvents. *J. Phys. Chem. A* **114**, 8345–8350 (2010).
66. Amaro, M., Birch, D. J. S. & Rolinski, O. J. Beta-amyloid oligomerisation monitored by intrinsic tyrosine fluorescence. *Phys. Chem. Chem. Phys.* **13**, 6434–6441 (2011).
67. Hsu, J. C.-C. *et al.* Thioflavin T and its photoirradiative derivatives: exploring their spectroscopic properties in the absence and presence of amyloid fibrils. *J. Phys. Chem. B* **117**, 3459–3468 (2013).
68. Khurana, R. *et al.* Mechanism of thioflavin T binding to amyloid fibrils. *Journal of Structural Biology* vol. 151 229–238 (2005).
69. Erez, Y., Liu, Y.-H., Amdursky, N. & Huppert, D. Modeling the nonradiative decay rate of electronically excited thioflavin T. *J. Phys. Chem. A* **115**, 8479–8487 (2011).
70. Fonin, A. V., Sulatskaya, A. I., Kuznetsova, I. M. & Turoverov, K. K. Fluorescence of dyes in solutions with high absorbance. Inner filter effect correction. *PLoS One* **9**, e103878 (2014).
71. Hasecke, F. *et al.* Origin of metastable oligomers and their effects on amyloid fibril self-assembly. *Chem. Sci.* **9**, 5937–5948 (2018).
72. Boulet-Audet, M., Vollrath, F. & Holland, C. Identification and classification of silks using infrared spectroscopy. *J. Exp. Biol.* **218**, 3138–3149 (2015).
73. Dyakonov, T. *et al.* Design and characterization of a silk-fibroin-based drug delivery platform using naproxen as a model drug. *J. Drug Deliv.* **2012**, 490514 (2012).
74. Sparkes, J. & Holland, C. Analysis of the pressure requirements for silk spinning reveals a pultrusion dominated process. *Nat. Commun.* **8**, 594 (2017).
75. LeVine, H. [18] Quantification of β-sheet amyloid fibril structures with thioflavin T. *Methods in Enzymology* 274–284 (1999) doi:10.1016/s0076-6879(99)09020-5.

76. Hagn, F., Thamm, C., Scheibel, T. & Kessler, H. pH-Dependent Dimerization and Salt-Dependent Stabilization of the N-terminal Domain of Spider Dragline Silk-Implications for Fibre Formation. *Angewandte Chemie International Edition* vol. 50 310–313 (2011).

77. Kronqvist, N. *et al.* Sequential pH-driven dimerization and stabilization of the N-terminal domain enables rapid spider silk formation. *Nat. Commun.* **5**, 3254 (2014).

Supplementary Materials

Full factorial ANOVA results

General Factorial Regression: Transition time Steepness of reaction versus silk and ThT concentration (Fluorescence)

Method:
Box-Cox transformation
Rounded λ -1
Estimated λ -0.945415
95% CI for λ (*, 1.75709)

Factor Information

Factor	Levels	Values
silk concentration	4	2, 3, 4, 5
Tht concentration	5	0, 20, 50, 100, 300

Analysis of Variance for Transformed Response

Source	DF	Adj SS	Adj MS	F-Value	P-Value
Model	7	0.000000	0.000000	10.49	0.000
Linear	7	0.000000	0.000000	10.49	0.000
silk concentration	**3**	**0.000000**	**0.000000**	**8.98**	**0.002**
Tht concentration	**4**	**0.000000**	**0.000000**	**11.62**	**0.000**
Error	12	0.000000	0.000000		
Total	19	0.000001			

Model Summary for Transformed Response

S	R-sq	R-sq(adj)	R-sq(pred)
0.0000770	85.95%	77.76%	60.98%

General Factorial Regression: Steepness of reaction versus silk and ThT concentration (Fluorescence)

Method:
Box-Cox transformation
Rounded λ 1
Estimated λ 0.880772
95% CI for λ (0.378272, 1.54727)

Factor Information

Factor	Levels	Values
silk concentration	4	2, 3, 4, 5
Tht concentration	5	0, 20, 50, 100, 300

Analysis of Variance

Source	DF	Adj SS	Adj MS	F-Value	P-Value
Model	7	0.002879	0.000411	11.58	0.000
Linear	7	0.002879	0.000411	11.58	0.000
silk concentration	3	0.000180	0.000060	1.69	0.222
Tht concentration	**4**	**0.002699**	**0.000675**	**19.00**	**0.000**
Error	12	0.000426	0.000036		
Total	19	0.003305			

Model Summary

S	R-sq	R-sq(adj)	R-sq(pred)
0.0059594	87.11%	79.59%	64.19%

General Factorial Regression: Maximum intensity versus silk and ThT concentration (Fluorescence)

Method:
Box-Cox transformation
Rounded λ -0.306999
Estimated λ -0.306999
95% CI for λ (-0.431499, -0.151499)

Factor Information

Factor	Levels	Values
silk concentration	4	2, 3, 4, 5
Tht concentration	5	0, 20, 50, 100, 300

Analysis of Variance for Transformed Response

Source	DF	Adj SS	Adj MS	F-Value	P-Value
Model	7	0.250621	0.035803	747.22	0.000
Linear	7	0.250621	0.035803	747.22	0.000
silk concentration	**3**	**0.004549**	**0.001516**	**31.65**	**0.000**
Tht concentration	**4**	**0.246071**	**0.061518**	**1283.90**	**0.000**
Error	12	0.000575	0.000048		
Total	19	0.251196			

Model Summary for Transformed Response

S	R-sq	R-sq(adj)	R-sq(pred)
0.0069220	99.77%	99.64%	99.36%

General Factorial Regression: Lag phase versus silk and ThT concentration (Fluorescence)

Method:
Box-Cox transformation
Rounded λ 0.5
Estimated λ 0.294582
95% CI for λ (*, 3.49508)

Factor Information

Factor	Levels	Values
silk concentration	4	2, 3, 4, 5
Tht concentration	5	0, 20, 50, 100, 300

Analysis of Variance for Transformed Response

Source	DF	Adj SS	Adj MS	F-Value	P-Value
Model	7	40.51	5.787	4.47	0.012
Linear	7	40.51	5.787	4.47	0.012
silk concentration	3	17.97	5.990	4.63	0.023
Tht concentration	4	22.54	5.634	4.35	0.021
Error	12	15.53	1.294		
Total	19	56.04			

Model Summary for Transformed Response

S	R-sq	R-sq(adj)	R-sq(pred)
1.13768	72.28%	56.12%	23.01%

General Factorial Regression: First transition versus silk and ThT concentration (Fluorescence)

Method:
Box-Cox transformation
Rounded λ -0.5
Estimated λ -0.573858
95% CI for λ (-1.00236, -0.136358)

Factor Information

Factor	Levels	Values
silk concentration	4	2, 3, 4, 5
Tht concentration	5	0, 20, 50, 100, 300

Analysis of Variance for Transformed Response

Source	DF	Adj SS	Adj MS	F-Value	P-Value
Model	7	0.000067	0.000010	87.22	0.000
Linear	7	0.000067	0.000010	87.22	0.000
silk concentration	**3**	**0.000064**	**0.000021**	**194.15**	**0.000**
Tht concentration	**4**	**0.000003**	**0.000001**	**7.03**	**0.004**
Error	12	0.000001	0.000000		
Total	19	0.000068			

Model Summary for Transformed Response

S	R-sq	R-sq(adj)	R-sq(pred)
0.0003317	98.07%	96.95%	94.65%

General Factorial Regression: Rate of the first transition versus silk and ThT concentration (Fluorescence)

Method:
Box-Cox transformation
Rounded λ -0.5
Estimated λ -0.431613
95% CI for λ (-0.916113, 0.00588736)

Factor Information

Factor	Levels	Values
silk concentration	4	2, 3, 4, 5
Tht concentration	5	0, 20, 50, 100, 300

Analysis of Variance for Transformed Response

Source	DF	Adj SS	Adj MS	F-Value	P-Value
Model	7	0.001664	0.000238	53.85	0.000
Linear	7	0.001664	0.000238	53.85	0.000
silk concentration	**3**	**0.001622**	**0.000541**	**122.51**	**0.000**
Tht concentration	4	0.000042	0.000010	2.36	0.112
Error	12	0.000053	0.000004		
Total	19	0.001717			

Model Summary for Transformed Response

S	R-sq	R-sq(adj)	R-sq(pred)
0.0021008	96.91%	95.12%	91.43%

General Factorial Regression: Lag phase versus silk and ThT concentration (Turbidity)

Method:
Box-Cox transformation
Rounded λ -0.5
Estimated λ -0.554124
95% CI for λ (-0.997624, -0.0986242)

Factor Information

Factor	Levels	Values
silk concentration	4	2, 3, 4, 5
Tht concentration	5	0, 20, 50, 100, 300

Analysis of Variance for Transformed Response

Source	DF	Adj SS	Adj MS	F-Value	P-Value
Model	7	0.000072	0.000010	63.88	0.000
Linear	7	0.000072	0.000010	63.88	0.000
silk concentration	**3**	**0.000068**	**0.000023**	**140.60**	**0.000**
Tht concentration	**4**	**0.000004**	**0.000001**	**6.34**	**0.006**
Error	12	0.000002	0.000000		
Total	19	0.000074			

Model Summary for Transformed Response

S	R-sq	R-sq(adj)	R-sq(pred)
0.0004026	97.39%	95.86%	92.74%

General Factorial Regression: Initial Push (raw voltage) versus silk and ThT concentration (Extrusion studies)

Method:
Box-Cox transformation
Rounded λ 1
Estimated λ 1.36723
95% CI for λ (-0.187268, 2.69573)

Factor Information

Factor	Levels	Values
silk concentration	4	2, 3, 4, 5
Tht concentration	5	0, 20, 50, 100, 300

Analysis of Variance

Source	DF	Adj SS	Adj MS	F-Value	P-Value
Model	7	6.04766	0.86395	17.51	0.000
Linear	7	6.04766	0.86395	17.51	0.000
silk concentration	3	5.95143	1.98381	40.22	0.000
Tht concentration	4	0.09623	0.02406	0.49	0.745
Error	12	0.59195	0.04933		
Total	19	6.63961			

Model Summary

S	R-sq	R-sq(adj)	R-sq(pred)
0.222102	91.08%	85.88%	75.23%

General Factorial Regression: Magnitude of the drop (raw voltage) versus silk and ThT concentration (Extrusion studies)

Method:
Box-Cox transformation
Rounded λ 2
Estimated λ 1.67488
95% CI for λ (0.999383, 2.52138)

Factor Information

Factor	Levels	Values
silk concentration	4	2, 3, 4, 5
Tht concentration	5	0, 20, 50, 100, 300

Analysis of Variance for Transformed Response

Source	DF	Adj SS	Adj MS	F-Value	P-Value
Model	7	87.325	12.4750	14.86	0.000
Linear	7	87.325	12.4750	14.86	0.000
silk concentration	3	84.606	28.2021	33.58	0.000
Tht concentration	4	2.719	0.6796	0.81	0.543
Error	12	10.077	0.8398		
Total	19	97.402			

Model Summary for Transformed Response

S	R-sq	R-sq(adj)	R-sq(pred)
0.916389	89.65%	83.62%	71.26%

General Factorial Regression: Slope of drop (raw voltage) versus silk and ThT concentration (Extrusion studies)

Method:
Box-Cox transformation
Rounded λ 0
Estimated λ 0.0556027
95% CI for λ (-0.306897, 0.436103)

Factor Information

Factor	Levels	Values
silk concentration	4	2, 3, 4, 5
Tht concentration	5	0, 20, 50, 100, 300

Analysis of Variance for Transformed Response

Source	DF	Adj SS	Adj MS	F-Value	P-Value
Model	7	13.5685	1.9384	7.06	0.002
Linear	7	13.5685	1.9384	7.06	0.002
silk concentration	3	12.6643	4.2214	15.37	0.000
Tht concentration	4	0.9041	0.2260	0.82	0.535
Error	12	3.2953	0.2746		
Total	19	16.8637			

Model Summary for Transformed Response

S	R-sq	R-sq(adj)	R-sq(pred)
0.524028	80.46%	69.06%	45.72%

General Factorial Regression: center of mass Amide I versus silk and ThT concentration (FTIR)

Method:
Box-Cox transformation
Rounded λ 0
Estimated λ -0.0894367
95% CI for λ (*, *)

Factor Information

Factor	Levels	Values
silk concentration	4	2, 3, 4, 5
Tht concentration	5	0, 20, 50, 100, 300

Analysis of Variance for Transformed Response

Source	DF	Adj SS	Adj MS	F-Value	P-Value
Model	7	0.000000	0.000000	4.03	0.017
Linear	7	0.000000	0.000000	4.03	0.017
silk concentration	3	0.000000	0.000000	9.24	0.002
Tht concentration	4	0.000000	0.000000	0.13	0.968
Error	12	0.000000	0.000000		
Total	19	0.000000			

Model Summary for Transformed Response

S	R-sq	R-sq(adj)	R-sq(pred)
0.0000501	70.18%	52.78%	17.16%

General Factorial Regression: center of mass Amide I versus silk and ThT concentration (FTIR)

Method:
Box-Cox transformation
Rounded λ 21
Estimated λ 21.4037
95% CI for λ (13.3492, 32.1732)

Factor Information

Factor	Levels	Values
silk concentration	4	2, 3, 4, 5
Tht concentration	5	0, 20, 50, 100, 300

Analysis of Variance for Transformed Response

Source	DF	Adj SS	Adj MS	F-Value	P-Value
Model	7	14641	2092	1.05	0.446
Linear	7	14641	2092	1.05	0.446
silk concentration	3	7538	2513	1.27	0.330
Tht concentration	4	7104	1776	0.90	0.497
Error	12	23807	1984		
Total	19	38448			

Model Summary for Transformed Response

S	R-sq	R-sq(adj)	R-sq(pred)
44.5409	38.08%	1.96%	0.00%

General Factorial Regression: Young modulus (MPa) versus silk and ThT concentration (Large-strain indentation)

Method:
Box-Cox transformation
Rounded λ 0.5
Estimated λ 0.613384
95% CI for λ (0.395884, 0.819884)

Factor Information

Factor	Levels	Values
silk concentration	4	2, 3, 4, 5
Tht concentration	5	0, 20, 50, 100, 300

Analysis of Variance for Transformed Response

Source	DF	Adj SS	Adj MS	F-Value	P-Value
Model	7	0.157497	0.022500	136.96	0.000
Linear	7	0.157497	0.022500	136.96	0.000
silk concentration	3	0.155997	0.051999	316.52	0.000
Tht concentration	4	0.001500	0.000375	2.28	0.120
Error	12	0.001971	0.000164		
Total	19	0.159469			

Model Summary for Transformed Response

S	R-sq	R-sq(adj)	R-sq(pred)
0.0128173	98.76%	98.04%	96.57%

General Factorial Regression: Shear modulus (MPa) versus silk and ThT concentration (Large-strain indentation)

Method:
Box-Cox transformation
Rounded λ 0.5
Estimated λ 0.672811
95% CI for λ (0.406311, 0.933311)

Factor Information

Factor	Levels	Values
silk concentration	4	2, 3, 4, 5
Tht concentration	5	0, 20, 50, 100, 300

Analysis of Variance for Transformed Response

Source	DF	Adj SS	Adj MS	F-Value	P-Value
Model	7	0.049129	0.007018	61.18	0.000
Linear	7	0.049129	0.007018	61.18	0.000
silk concentration	3	0.048738	0.016246	141.63	0.000
Tht concentration	4	0.000391	0.000098	0.85	0.519
Error	12	0.001377	0.000115		
Total	19	0.050505			

Model Summary for Transformed Response

S	R-sq	R-sq(adj)	R-sq(pred)
0.0107103	97.27%	95.68%	92.43%

Extrusion (raw data):

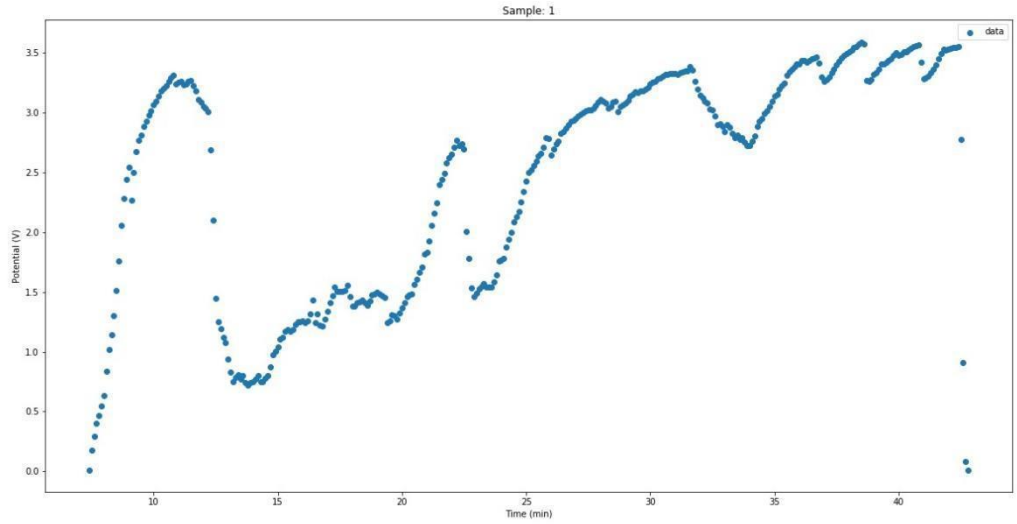

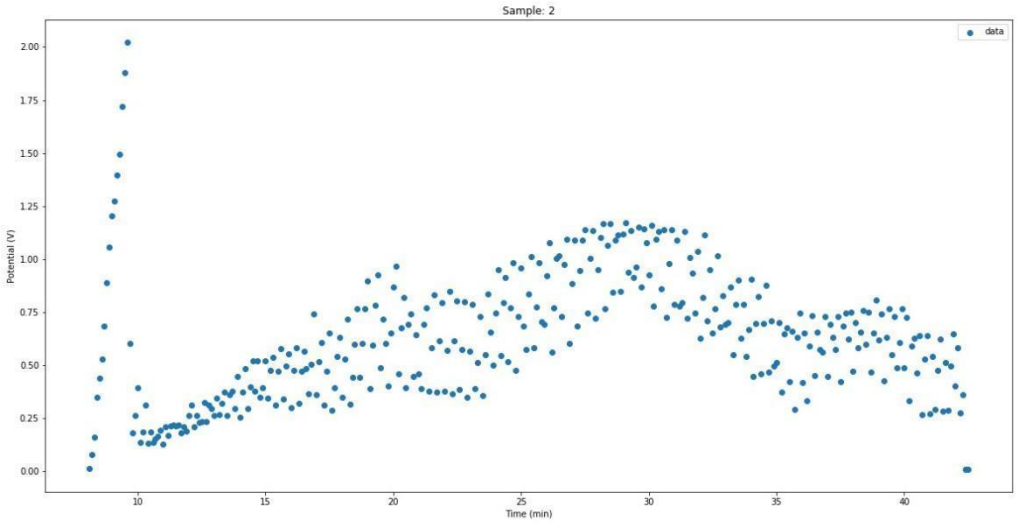

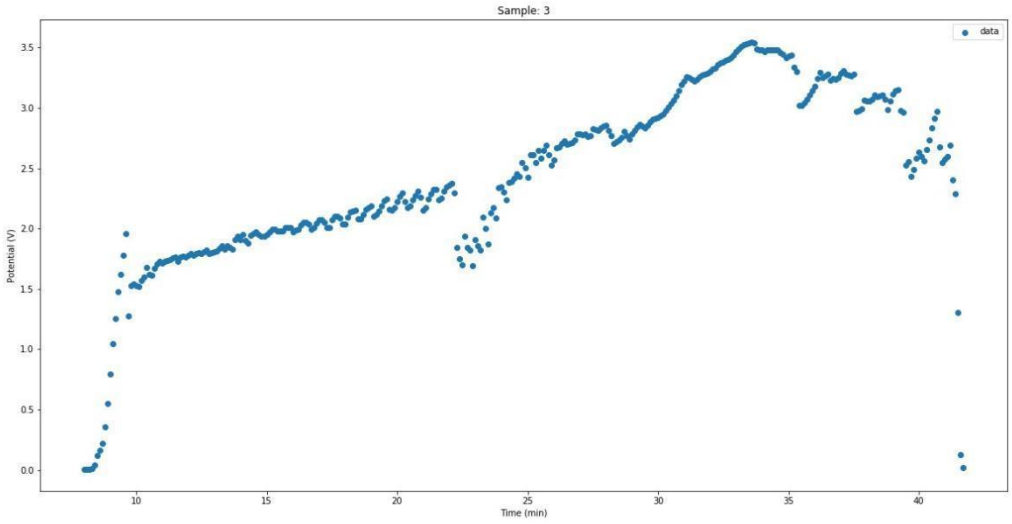
Sample: 3
data
Potential (V)
Time (min)

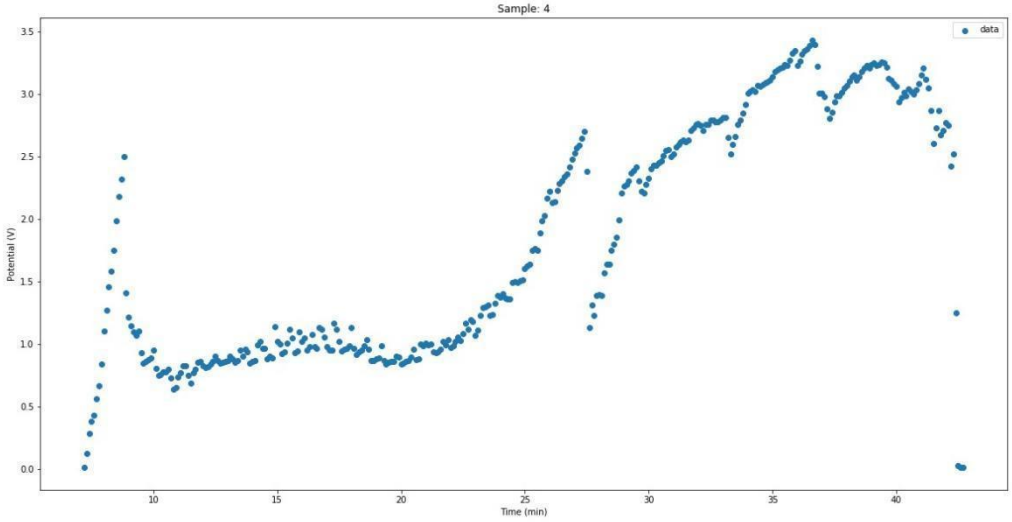
Sample: 4
data
Potential (V)
Time (min)

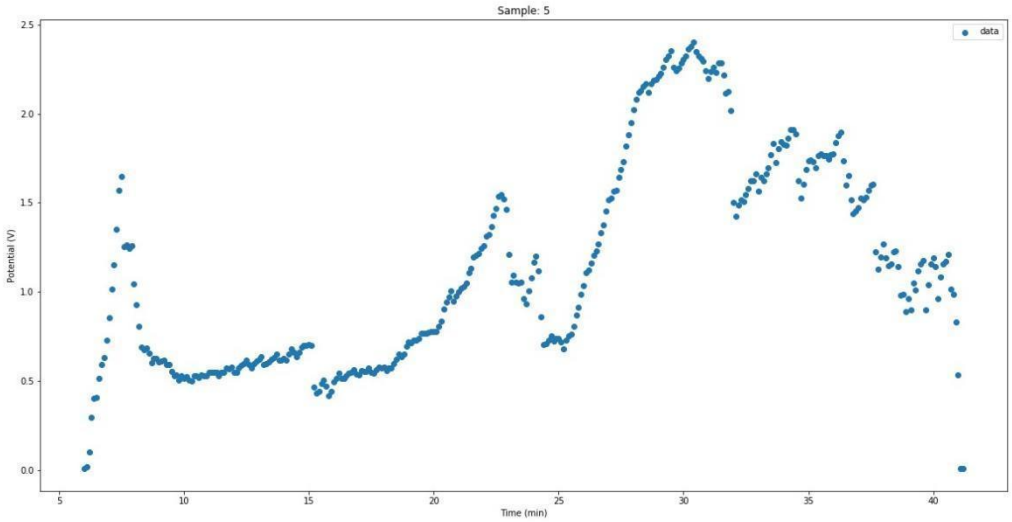
Sample: 5
data
Potential (V)
Time (min)

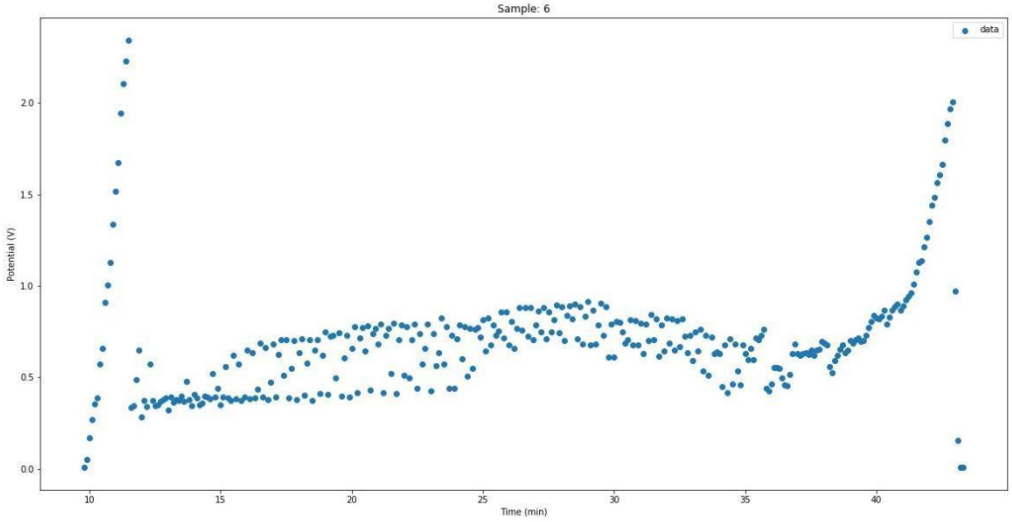
Sample: 6
data
Potential (V)
Time (min)

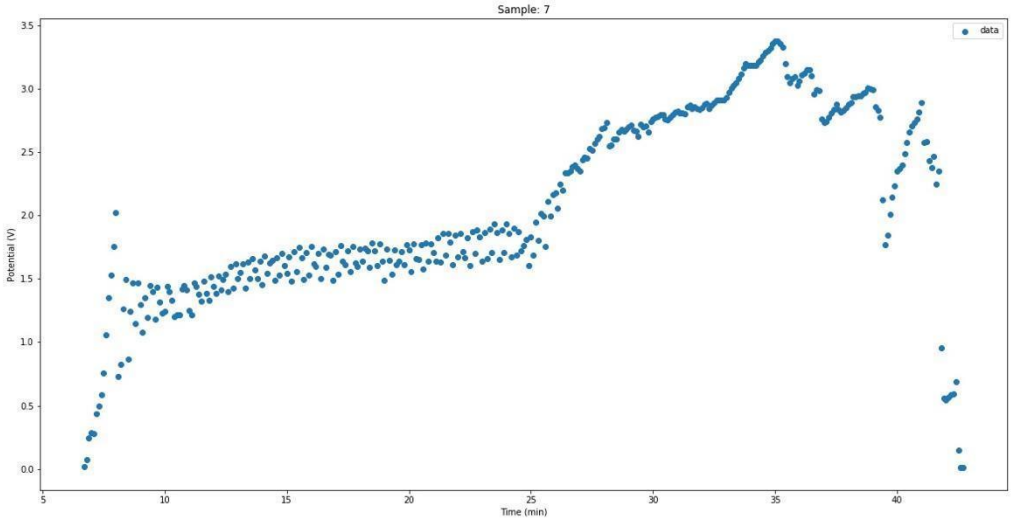
Sample: 7
data
Potential (V)
Time (min)

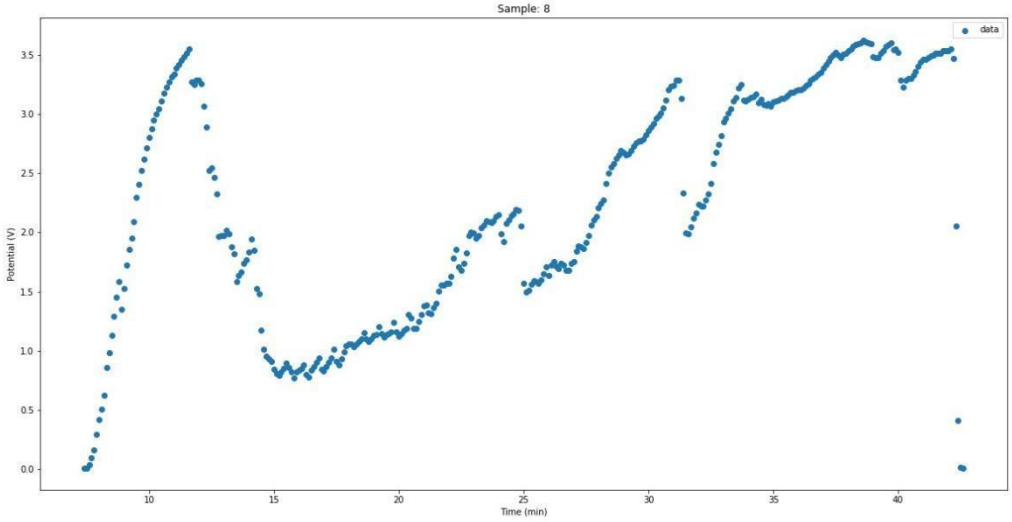
Sample: 8
data
Potential (V)
Time (min)

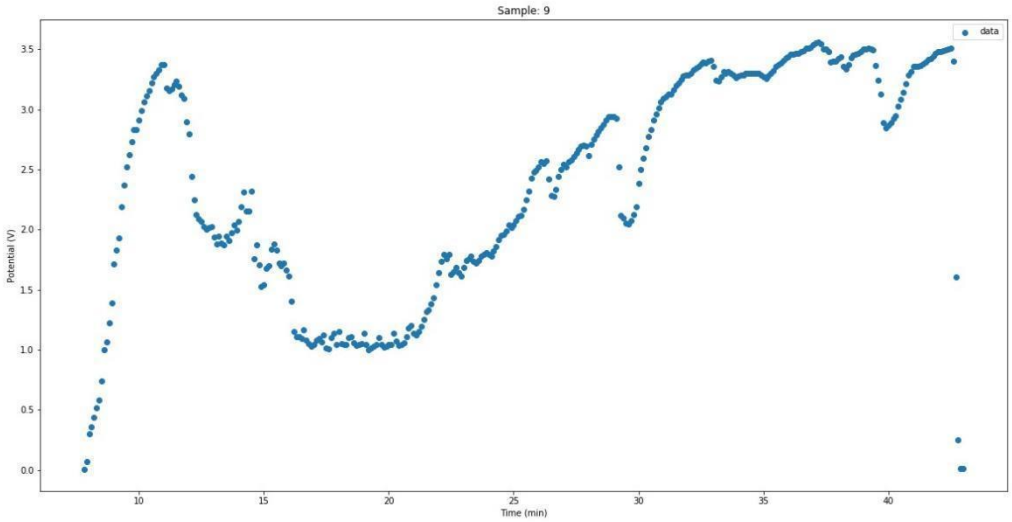
Sample: 9
data
Potential (V)
Time (min)

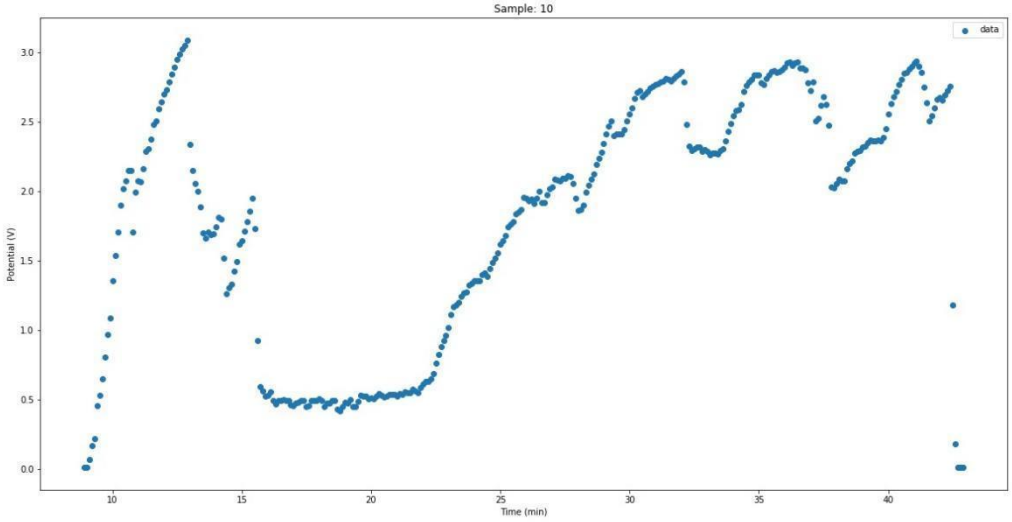
Sample: 10
data
Potential (V)
Time (min)

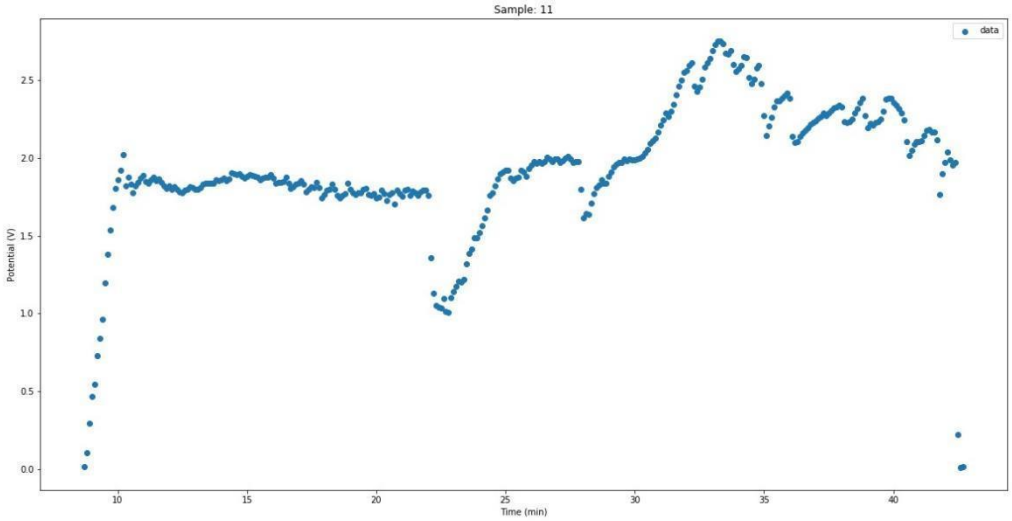
Sample: 11
data
Potential (V)
Time (min)

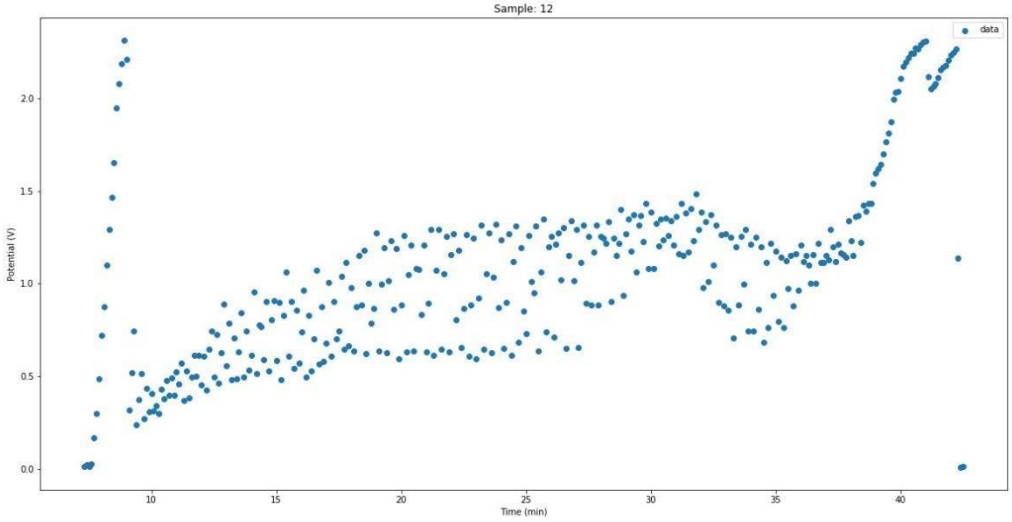
Sample: 12
data
Potential (V)
Time (min)

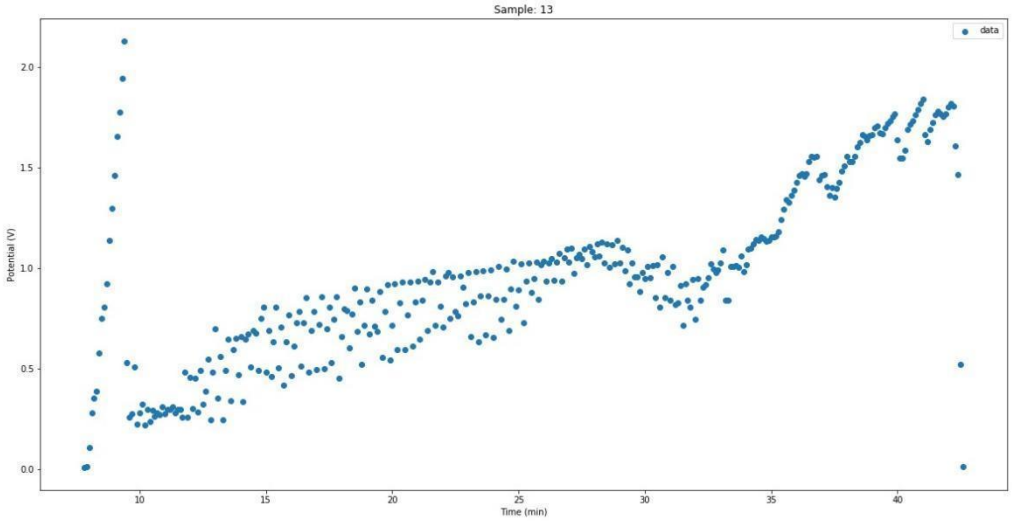
Sample: 13
data
Potential (V)
Time (min)

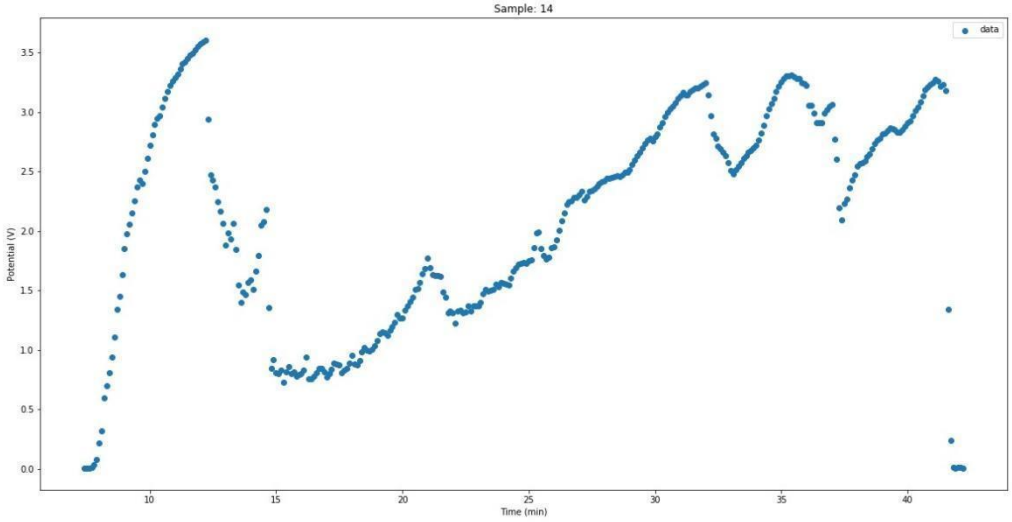
Sample: 14
data
Potential (V)
Time (min)

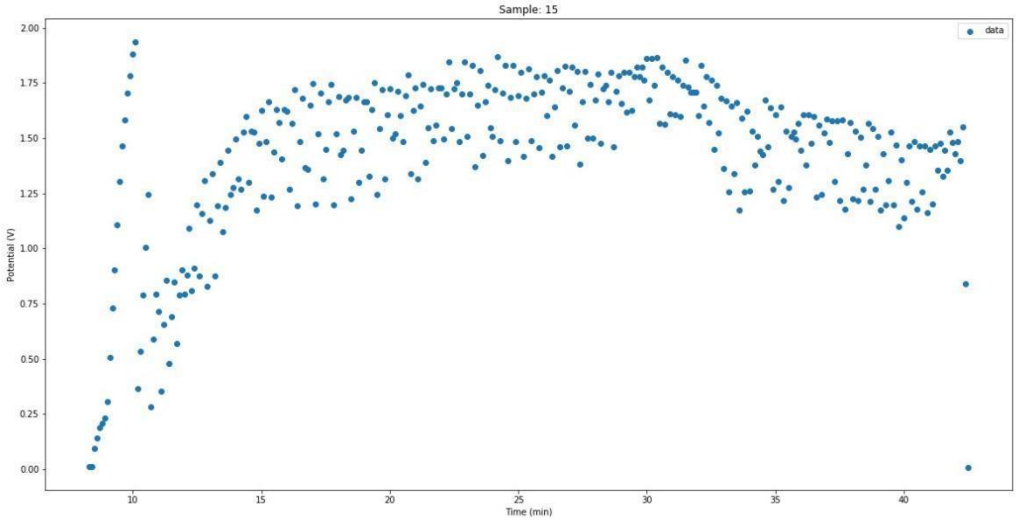
Sample: 15
data
Potential (V)
Time (min)

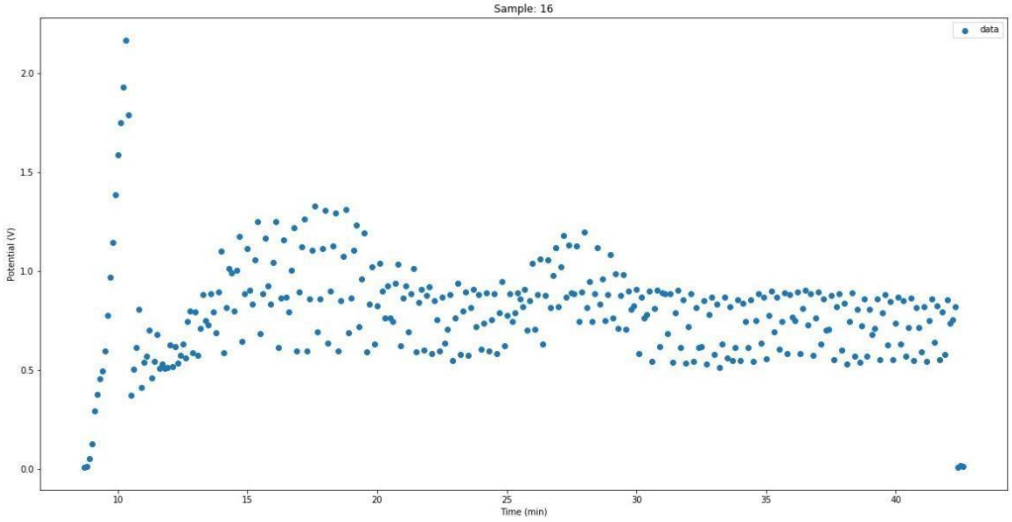
Sample: 16
data
Potential (V)
Time (min)

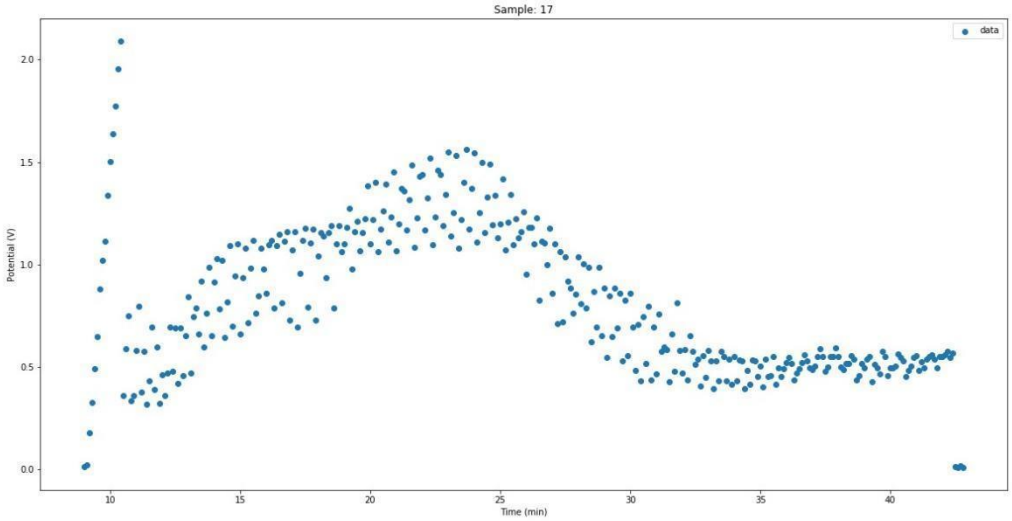
Sample: 17
data
Potential (V)
Time (min)

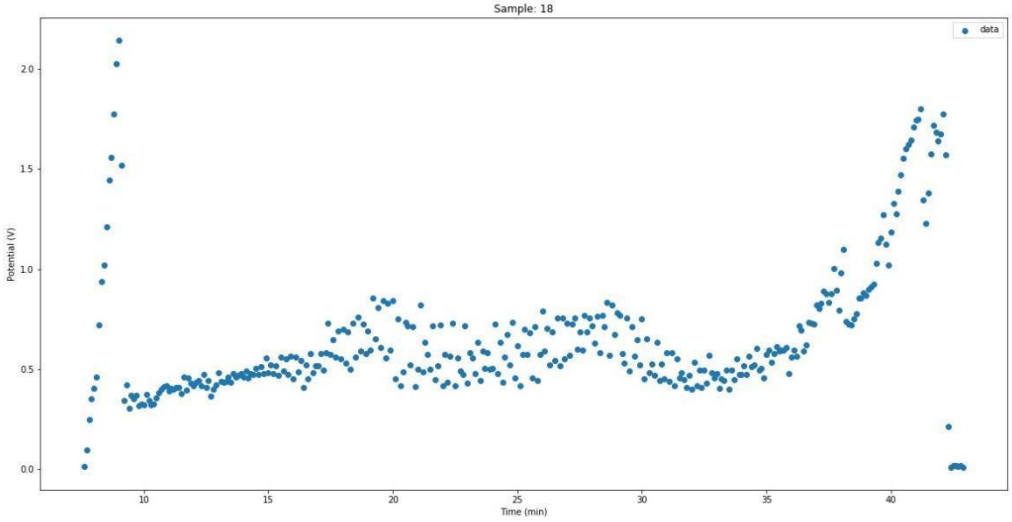
Sample: 18
data
Potential (V)
Time (min)

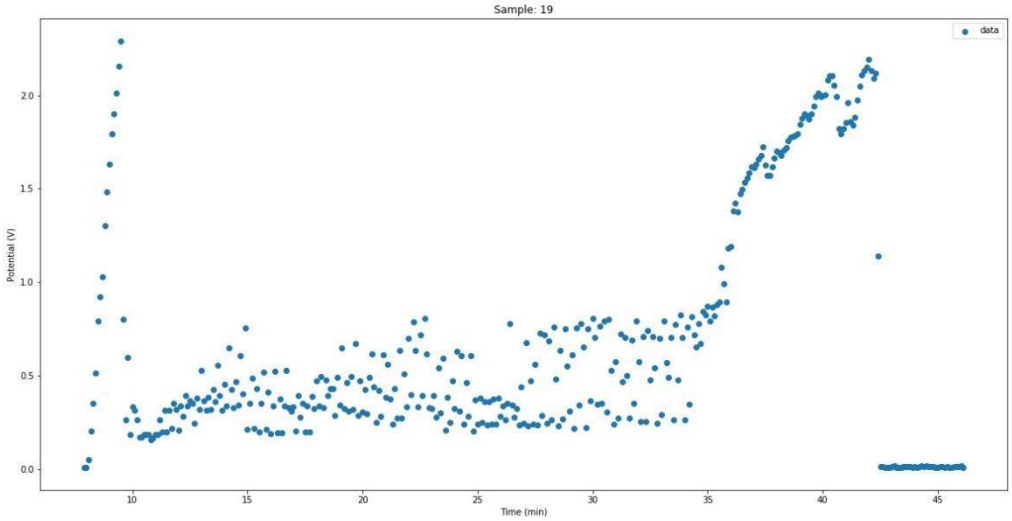
Sample: 19
data
Potential (V)
Time (min)

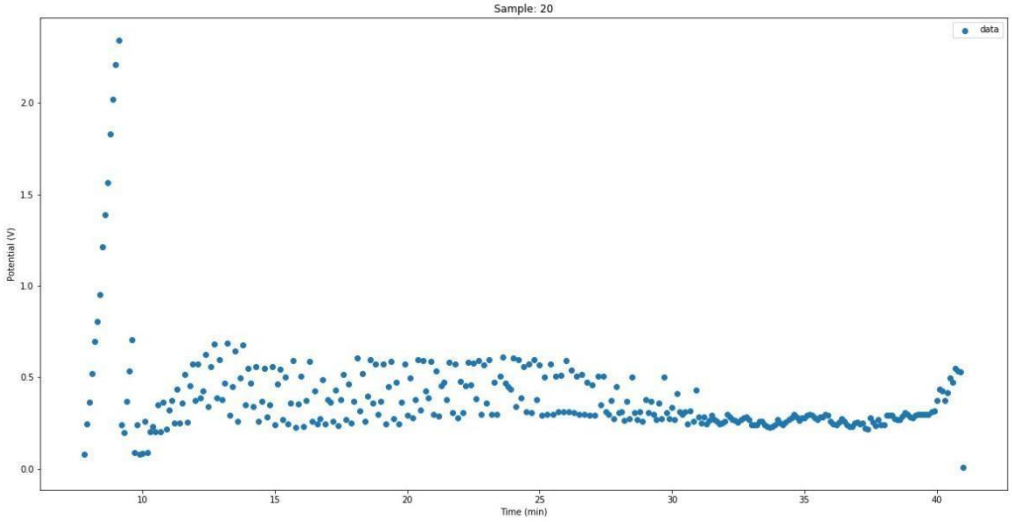
Sample: 20
data
Potential (V)
Time (min)